targeting motif distal to the dileucine signal. Biochem J 350:99–107
28. Piper RC, Tai C, Kulesza P, Pang S, Warnock D, Baenziger J, Slot JW, Geuze HJ, Puri C, James DE 1993 GLUT4 NH2 terminus contains a phenylalanine-based targeting motif that regulates intracellular sequestration. J Cell Biol 121:1221–1232
29. Bunn RC, Jensen MA, Reed BC 1999 Protein interactions with the glucose transporter binding protein GLUT1CBP that provide a link between GLUT1 and the cytoskeleton. Mol Biol Cell 10:819–832
30. Songyang Z, Fanning AS, Fu C, Xu J, Marfatia SM, Chishti AH, Crompton A, Chan AC, Anderson JM, Cantley LC 1997 Recognition of unique carboxy-terminal motifs by distinct PDZ domains. Science 275:73–77
31. Brown D, Rose J 1991 Sorting of GPI-anchored protein to glycolipid-enriched membrane subdomains during transport to the apical cell surface. Cell 68:533–544
32. Sakyo T, Kitagawa T 2002 Differential localization of glucose transporter isoforms in non-polarized mammalian cells: distribution of GLUT1 but not GLUT3 to detergent-resistant membrane domains. Biochim Biophys Acta 1567:165–175
33. Jolimay N, Franck L, Langlois X, Hamon M, Darmon M 2000 Dominant role of the cytosolic C-terminal domain of the rat 5-HT1B receptor in axonal-apical targeting. J Neurosci 20:9111–9118
34. Tugizov S, Maidji E, Xiao J, Zheng Z, Pereira L 1998 Human cytomegalovirus glycoprotein B contains autonomous determinants for vectorial targeting to apical membranes of polarized epithelial cells. J Virol 72: 7374–7386
35. Milewski MI, Mickle, JE, Forrest JK, Stafford DM, Moyer BD, Cheng J, Guggino WB, Stanton BA, Cutting GR 2001 A PDZ-binding motif is essential but not sufficient to localize the C terminus of CFTR to the apical membrane. J Cell Sci 114:719–726
36. Sun AQ, Salkar R, Xu SS, Zeng L, Zhou MM, Suchy FJ 2003 A 14-amino acid sequence with a β-turn structure is required for apical membrane sorting of the rat ileal bile acid transporter. J Biol Chem 278:4000–4009
37. Chuang JZ, Sung CH 1998 The cytoplasmic tail of rhodopsin acts as a novel apical sorting signal in polarized MDCK cells. J Cell Biol 142:1245–1256
38. Heijnen HF, Oorschot V, Sixma JJ, Slot JW, James DE 1997 Thrombin stimulates glucose transport in human platelet via translocation of the glucose transporter GLUT3 from α-granules to the cell surface. J Cell Biol 138:323–330
39. Angulo C, Rauch MC, Droppelmann A, Reyers AM, Slebe JC, Delgado-Lopez F, Guaiquil VH, Vera JC, Concha II 1998 Hexose transporter expression and function in mammalian spermatozoa: cellular localization and transport of hexoses and vitamin C. J Cell Biochem 71: 189–203
40. Thoidis G, Kupriyanova T, Cunningham JM, Chen P, Cadel S, Foulon T, Cohen P, Fine RE, Kandror KV 1999 Glucose transporter GLUT3 is targeted to secretory vesicles in neurons and PC12 cells. J Biol Chem 274: 14062–14066
41. Dotti CG, Simons K 1990 Polarized sorting of viral glycoproteins to the axon and dendrites of hippocampal neurons in culture. Cell 62:63–72
42. Katagiri H, Asano T, Ishihara H, Tsukuda K, Lin JL, Inukai K, Kikuchi M, Yazaki Y, Oka Y 1992 Replacement of intracellular C-terminal domain of GLUT1 glucose transporter with that of GLUT2 increases V_{max} and K_m of transport activity. J Biol Chem 267:22550–22555
43. Inukai K, Asano T, Katagiri H, Ishihara H, Anai M, Fukushima Y, Tsukuda K, Kikuchi M, Yazaki Y, Oka Y 1993 Cloning and increased expression with fructose feeding of rat jejunal GLUT5. Endocrinology 133: 2009–2014

Molecular Endocrinology **is published monthly by The Endocrine Society (http://www.endo-society.org), the foremost professional society serving the endocrine community.**

Available online at www.sciencedirect.com
SCIENCE DIRECT®
Biochemical and Biophysical Research Communications 325 (2004) 250–256
BBRC
www.elsevier.com/locate/ybbrc

Endoplasmic reticulum stress and N-glycosylation modulate expression of WFS1 protein

Suguru Yamaguchi[a], Hisamitsu Ishihara[a,*], Akira Tamura[a], Takahiro Yamada[a], Rui Takahashi[a], Daisuke Takei[a], Hideki Katagiri[b], Yoshitomo Oka[a]

[a] *Division of Molecular Metabolism and Diabetes, Tohoku University Graduate School of Medicine, 2-1 Seiryo-machi, Aoba-ku, Sendai, Miyagi 980-8575, Japan*
[b] *Division of Advanced Therapeutics for Metabolic Diseases, Tohoku University Graduate School of Medicine, 2-1 Seiryo-machi, Aoba-ku, Sendai, Miyagi 980-8575, Japan*

Received 22 September 2004
Available online 22 October 2004

Abstract

Mutations of the *WFS1* gene are responsible for two hereditary diseases, Wolfram syndrome and low frequency sensorineural hearing loss. The WFS1 protein is a glycoprotein located in the endoplasmic reticulum (ER) membrane but its function is poorly understood. Herein we show WFS1 mRNA and protein levels in pancreatic islets to be increased with ER-stress inducers, thapsigargin and dithiothreitol. Another ER-stress inducer, the N-glycosylation inhibitor tunicamycin, also raised WFS1 mRNA but not protein levels. Site-directed mutagenesis showed both Asn-663 and Asn-748 to be N-glycosylated in mouse WFS1 protein. The glycosylation-defective WFS1 protein, in which Asn-663 and Asn-748 had been substituted with aspartate, exhibited an increased protein turnover rate. Consistent with this, the WFS1 protein was more rapidly degraded in the presence of tunicamycin. These data indicate that ER-stress and N-glycosylation play important roles in WFS1 expression and stability, and also suggest regulatory roles for this protein in ER-stress induced cell death.

Keywords: Wolfram syndrome; Low frequency sensorineural hearing loss; WFSI; ER-stress; N-Glycosylation

The *WFS1* gene, encoding a transmembrane protein of the endoplasmic reticulum (ER) [1], is mutated in two hereditary diseases, autosomal recessive Wolfram syndrome (OMIN:222300) [2,3] and autosomal dominant low frequency sensorineural hearing loss (LFSNHL) (OMIM:600965) [4,5]. The former is also known as DIDMOAD, summarizing the most frequent symptoms; diabetes insipidus, diabetes mellitus, optic atrophy, and deafness. More than 100 mutations of the *WFS1* gene have been identified to date in patients with these diseases [6]. WFS1 protein, also called wolframin, consists of 890 amino acids [2,3] and its homologues are found in several organisms; *Drosophila melanogaster* (CG4917), *Anopheles gambiae* (EBIP3764), *Ciona intestinalis* (Cin.16116), *Fugu rubripes* (SINFRUP82345), and *Xenopus laevis* (Xl.3995). However, these proteins share no homology with known proteins, making it difficult to speculate as to their functions.

We recently established a murine model with a disrupted *wfs1* gene [7]. Mutant mice exhibited impaired glucose homeostasis due to defective insulin secretion in vivo. Studies using isolated islets revealed that mutant islet cells were prone to apoptosis induced by insults which impair ER functions and trigger the so-called unfolded protein response (UPR) [8,9]. Therefore, it was suggested that WFS1 protein plays a role in modulation of apoptotic processes that arise from impairment of ER function [7]. In addition, isolated islets from WFS1-deficient mice exhibited defective insulin

* Corresponding author. Fax: +81 22 717 7612.
E-mail address: ishihara-tky@umin.ac.jp (H. Ishihara).

0006-291X/$ - see front matter © 2004 Elsevier Inc. All rights reserved.
doi:10.1016/j.bbrc.2004.10.017

secretion which was accompanied by decreased calcium responses to glucose. Conversely, wolframin-overexpressing islets showed increased insulin secretion, indicating that wolframin also participates in regulation of stimulus-secretion coupling in insulin exocytosis [7]. It has recently been reported that WFS1 protein/wolframin expression in *Xenopus* oocytes conferred cation channel activity and increased cytosolic calcium levels [10]. This observation is intriguing since intracellular calcium regulation plays important roles in modulating both apoptotic and exocytotic processes. Despite these advancements, however, little is known about the mechanisms by which WFS1 protein actually alters these processes.

To understand the role that WFS1 protein/wolframin plays in the regulation of apoptotic and exocytotic events as well as in other as yet unknown cellular processes, information on the structure and function of this protein must be obtained. The amino acid sequence suggests that WFS1 protein is a multi-membrane spanning protein with hydrophilic amino (N)- and carboxy (C)-terminal regions [2,3]. In addition, biochemical and immunocytochemical analyses showed WFS1 protein to be an ER membrane glycoprotein [1].

In the present studies, we first examined WFS1 protein expression after treatment with agents that trigger UPR. We found WFS1 mRNA and protein levels to be increased by thapsigargin or dithiothreitol (DTT). Treatment with tunicamycin, an inhibitor of N-glycosylation, also raised WFS1 mRNA levels, suggesting that UPR increases WFS1 mRNA levels. However, the WFS1 protein level is not increased by tunicamycin. Subsequent analyses demonstrated protein stability to be reduced in the glycosylation-defective WFS1 protein. These results contribute to further understanding of the functions of this enigmatic protein.

Materials and methods

Reagents and antibodies. Tunicamycin, thapsigargin, DTT, and anti-actin antibody were purchased from Sigma–Aldrich Japan (Tokyo, Japan). Anti-HA and anti-CHOP antibodies were obtained from Santa Cruz Biotechnology (Santa Cruz, CA). Anti-WFS1 N-terminus antibody was described previously [11].

Pancreatic islet isolation and treatment with ER-stress inducers. Pancreatic islets were isolated from male C57BL/6 mice by retrograde injection of collagenase (Sigma–Aldrich Japan, Tokyo, Japan) into the pancreatic duct. Approximately 100 (for Western blot analyses) or 200 (for RNA extraction) islets were treated with 2 μg/ml thapsigargin, 5 mM DTT, or 5 μM tunicamycin for 36 h in RPMI1640 medium. Total RNA was extracted using Isogen reagent (NipponGene, Toyama, Japan). Quantitative real-time PCR analysis for WFS1 mRNA levels was performed using primers, 5′-CTGGAAACTCAACCCCAAGA-3′ and 5′-TTGGATTCACTGCTGACGAG-3′.

Plasmids. pHA-mWFS1 encodes a fusion protein consisting of an initiator methionine, the HA epitope tag (YPYDVPDYA), and amino acids 2–890 of mouse WFS1 protein. To generate this plasmid, a fragment encoding a *SalI* restriction site and amino acids 2–484 was amplified by PCR. Using the PCR method, pmWFS1-HA encoding mouse WFS1 protein with an HA tag between residues 830 and 831 was also generated. pHA-mWFS1(N633D) and pHA-mWFS1 (N748D), which encode HA-tagged WFS1 protein with a mutation of asparagine 633 to aspartate and asparagine 748 to aspartate, respectively, were generated using PCR-based mutagenesis on pHA-mWFS1. pHA-mWFS1(N633D/N748D) encoding a mutant protein with mutation of both asparagine residues was generated using pHA-mWFS1(N633D).

Cell culture and transient transfection. MIN6 [12] and COS7 cells were grown in Dulbecco's modified Eagle's medium (DMEM) supplemented with 10% (v/v) fetal calf serum, 50 U/ml penicillin, and 50 μg/ml streptomycin sulfate. Transfection of plasmids was carried out using FuGENE6 (Roche, Indianapolis, IN) diluted in OPTI media (Invitrogen, Carlsbad, CA). Cells were harvested for Western blot or proceeded to immunostaining analysis 36 h after transfection. Immunostaining was performed using anti-HA antibody and FITC-conjugated anti-mouse IgG (Jackson ImmunoResearch, West Grove, PA).

Trypsin treatment. COS7 cells transfected with either pHA-mWFS1 or pmWFS1-HA were homogenized in a buffer containing 270 mM sucrose, 2 mM EDTA, and 50 mM Hepes (pH 7.5). Cellular membranes were recovered by centrifuging the homogenate at 17,400*g* for 15 min. Membranes (100 μg) were then incubated with trypsin at various concentrations at 4 °C. After a 30 min incubation, homogenates were boiled and subjected to SDS/PAGE and Western blot analysis.

Endoglycosydase cleavage. COS7 cells transfected with either wild-type WFS1 cDNA or mutant constructs were dissolved in denaturing buffer (0.5% SDS, 1% β-mercaptoethanol), boiled for 10 min at 100 °C, then incubated at 37 °C for 1 h with endoglycosidase H (500 U), and subjected to electrophoresis on NuPAGE 3–8% Tris–acetate gel (Invitrogen).

Metabolic labeling. MIN6 cells were labeled with [^{35}S]methionine and [^{35}S]cysteine (100 μCi/ml; EXPRE^{35}S^{35}S labeling mix, Perkin–Elmer-New England Nuclear, Boston, MA) in DMEM with either methionine or cysteine in the presence or absence of 5 μg/ml tunicamycin for 3 h. Cells were then chased for different periods in complete medium with or without tunicamycin. COS7 cells transfected with pHA-mWFS1 or pHA-mWFS1(N633D/N748D) were also labeled with [^{35}S]methionine and [^{35}S]cysteine for 3 h. Cells were then chased for different periods in complete medium. MIN6 and COS7 cells were lysed in a buffer containing 100 mM NaCl, 0.5 mM EDTA, 20 mM Tris (pH 7.5), and 0.5% NP-40. Lysates were incubated with 10 μl protein A/G–Sepharose (Amersham Biosciences, Piscataway, NJ) for 2 h and then briefly centrifuged. The resulting supernatant was incubated with anti-WFS1 N-terminus or anti-HA antibodies overnight and then incubated with protein A/G–Sepharose for 2 h. The beads were washed three times and bound WFS1 proteins were eluted in SDS-sample buffer and subjected to SDS/PAGE (10%).

Statistical analyses. Data are presented as means ± SE. Differences were assessed by Student's *t* test.

Results and discussion

Effect of ER-stress inducers on WFS1 expression in pancreatic islets

We recently reported that WFS1-deficient islets exhibited increased susceptibility to apoptosis due to impaired ER function [7]. Therefore, in this study, we first determined WFS1 expression in isolated mouse pancreatic islets treated with the ER-stress inducers, thapsigargin, DTT, and tunicamycin. Thapsigargin is an inhibitor of the sarco(endo)plasmic reticulum Ca^{2+} pump and

depletes ER Ca^{2+}, which affects the functions of Ca^{2+}-dependent ER chaperone proteins. DTT and tunicamycin affect protein folding by disrupting disulfide bonds and inhibiting N-glycosylation, respectively. These compounds therefore cause mis-folding of proteins (ER-stress) and induce UPR [13]. As shown in Fig. 1, WFS1 protein expression was increased in islets treated with 2 μM thapsigargin (Fig. 1A) or 5 mM DTT (Fig. 1B) for 36 h. Greater than threefold increases in WFS1 mRNA levels were also observed by quantitative RT-PCR analyses in islets treated with these agents (data not shown). Another ER-stress inducer, tunicamycin (5 μg/ml), did not raise WFS1 protein levels in isolated islets (Fig. 1C). However, quantitative RT-PCR analyses revealed WFS1 mRNA levels to be increased by 72% in islets treated with tunicamycin (Fig. 1D). These data suggest that WFS1 mRNA expression increases in response to the ER-stress.

WFS1 protein has been shown to be a glycoprotein [1] like the inositol trisphosphate receptor, another ER membrane resident protein essential for cellular calcium homeostasis and signaling [14]. The unaltered WFS1 protein levels despite increased mRNA levels in islets treated with tunicamycin raise the possibility that inhibition of N-glycosylation affects WFS1 protein stability. To address this possibility, pancreatic β-cell derived MIN6 cells were labeled for 3 h with [^{35}S]methionine/cysteine and chased with unlabeled methionine and cysteine for different intervals in the continuous absence or presence of tunicamycin. As shown in Fig. 1E, WFS1 protein in tunicamycin-treated cells was more rapidly degraded, suggesting that inhibition of N-glycosylation reduces WFS1 protein stability.

Membrane topology of WFS1 protein

To study the roles of N-glycosylation more specifically, we first sought to determine N-glycosylation site(s) of WFS1 protein/wolframin. Since N-glycosylation occurs in the ER, it was prerequisite to know the membrane topology of this protein. The initial hydropathy plot studies did not provide a definitive answer; WFS1 protein contains 9 or 10 transmembrane segments, with long hydrophilic stretches on both the N- and the C-termini [2,3].

To localize the N- and the C-termini of WFS1 protein with respect to the ER membrane, we transiently expressed, in COS7 cells, mouse WFS1 protein tagged with an HA-epitope in either the N- or the C-terminal stretch (designated HA-mWFS1 or mWFS1-HA, respectively,

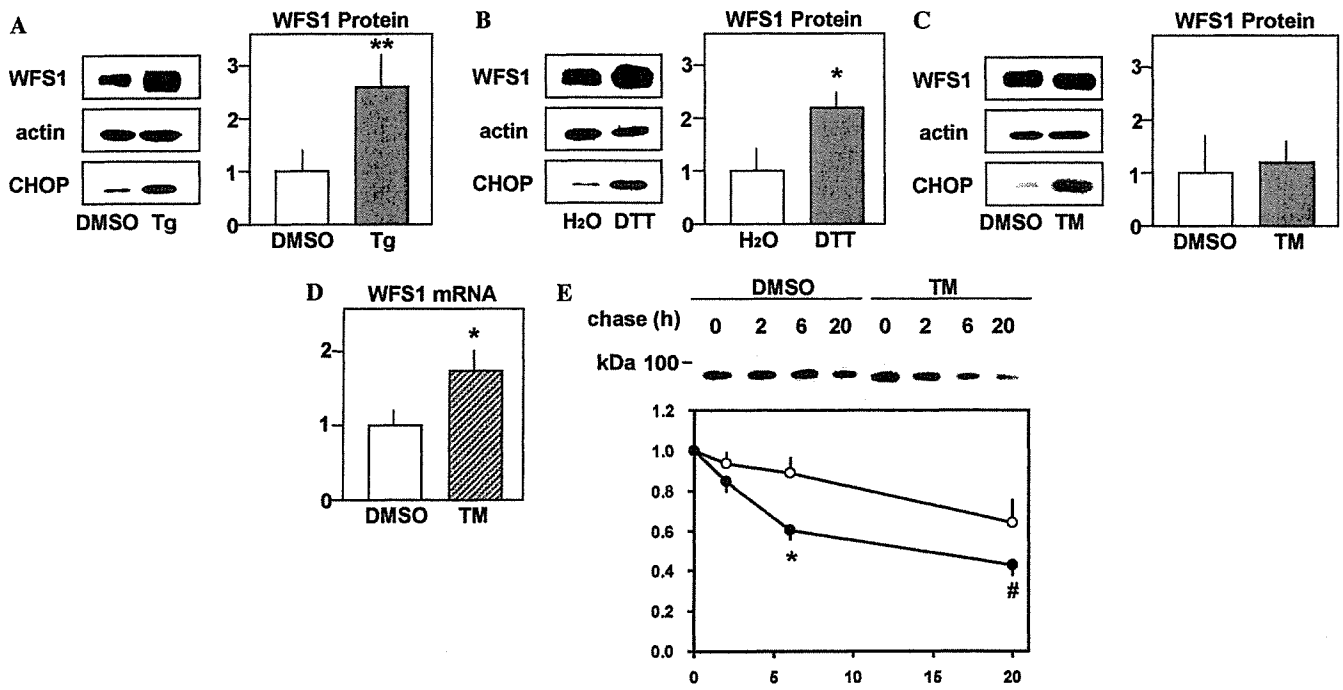

Fig. 1. WFS1 expression in mouse pancreatic islets in response to ER-stress inducers. (A–C) Isolated mouse islets were challenged with 2 μM thapsigargin (Tg) (A, $n = 4$), 5 mM DTT (B, $n = 3$) or 5 μg/ml tunicamycin (TM) (C, $n = 5$). After a 36-h incubation, the islets were subjected to SDS/PAGE and blotted using antibodies against the WFS1 N-terminus, actin, or CHOP. Representative blots are shown in the left panels. Increased CHOP expression indicated successful induction of ER-stress mediated apoptosis. WFS1 protein/actin levels are summarized in the right panels. Data are expressed as the expression relative to those of a control islet preparation. (D) Total RNA was extracted from isolated mouse islets treated with 5 μg/ml tunicamycin for 36 h. WFS1 and GAPDH mRNA levels were determined by quantitative real-time PCR. WFS1 mRNA levels were normalized to those of GAPDH. Data were obtained using three independent sets of islet preparations. (E) MIN6 cells were pulse-labeled for 3 h without or with 5 μg/ml tunicamycin and chased for up to 20 h in the continuous absence or presence of the drug. A representative result from three independent experiments is shown in the upper panel. Data from three experiments are summarized, after normalization to time zero of the chase in the lower panel. Open circles, DMSO-treated MIN6 cells. Closed circles, tunicamycin-treated cells. $^{\#}P = 0.0634$, $^{*}P < 0.05$, $^{**}P < 0.01$.

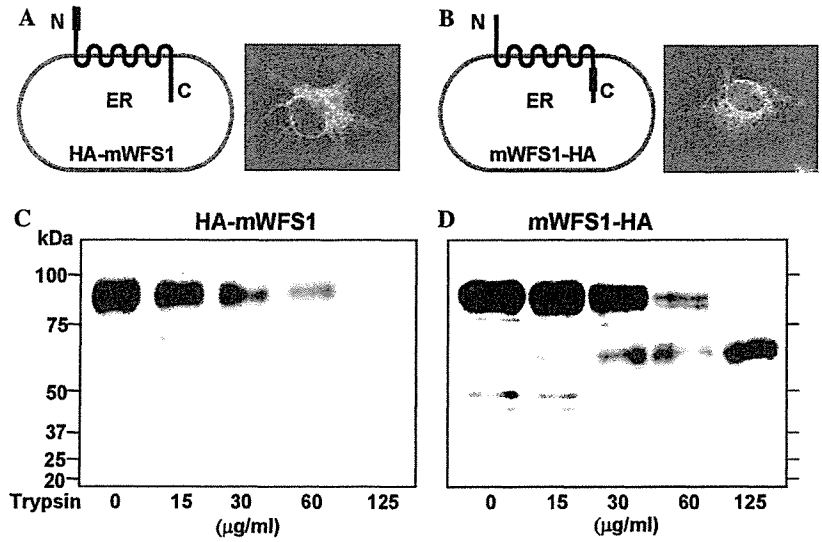

Fig. 2. Membrane orientations of the N- and the C-termini of WFS1 protein as determined by trypsin proteolysis. WFS1 protein tagged with the HA epitope at either the N- (A,C) or the C-terminus (B,D) was expressed in COS7 cells. (A,B) Schematic illustration and immunocytochemical demonstration of the HA-tagged WFS1 proteins used in (C) and (D). (C,D) Membranes from COS7 cells transfected with a plasmid encoding either HA-mWFS1 or mWFS1-HA were treated with the indicated amounts of trypsin. After incubation for 30 min at 4 °C, the reactions were stopped by boiling for 5 min, and subjected to SDS/PAGE and immunoblot analysis with anti-HA antibody.

Figs. 2A and B). HA-mWFS1 and mWFS1-HA proteins were successfully expressed and localized to the ER, as demonstrated by reticular staining in the cytoplasm (Figs. 2A and B). Membrane preparation of cells expressed with either HA-mWFS1 or mWFS1-HA proteins was then subjected to trypsin digestion followed by SDS/PAGE and immunoblotting with an antibody against the HA epitope. The HA-epitope tagged at the N-terminus was completely digested with increasing concentrations of trypsin (Fig. 2C). This was not due to loss of membrane vesicle integrity, since no changes in an ER-resident chaperone protein, GRP78, were detected using an antibody against GRP78 in the same membrane preparations (data not shown). In contrast, the C-terminal HA epitope was protected from trypsin (Fig. 2D). These results indicated that WFS1 protein has odd numbers of transmembrane segments with the orientation of the N-terminus toward the cytoplasm and that of the C-terminus toward the ER lumen. A similar conclusion was obtained by trypsin-digestion of the membrane, followed by detection with C-terminal or N-terminal antibodies [15].

Determination of N-glycosylation sites.

Mouse WFS1 protein has six asparagine residues with the consensus sequence for N-glycosylation (N-X-S/T, where X is any amino acid except for proline). According to a 9-transmembrane model with N-terminus cytosolic/C-terminus luminal orientation, asparagines 663 and 748 would be localized in the ER. Therefore, we mutated these two asparagine residues to aspartate in order to determine whether one or both are N-linked glycosylation site(s). Mutant WFS1 proteins in which asparagine 663 and/or asparagine 748 was mutated to aspartate [designated HA-mWFS1(N663D), HA-mWFS1(N748D), and HA-mWFS1(N663D/N748D)] were successfully expressed in the ER (Fig. 3A). When these WFS1 mutant proteins were subjected to SDS/PAGE, HA-mWFS1(N663D/N748D) migrated faster than the HA-wild-type mWFS1 protein, while both HA-mWFS1(N663D) and HA-mWFS1(N748D) mutants were between the two (Fig. 3B). These results suggested that both asparagine residues, 663 and 748, are glycosylation sites and place the C-terminal stretch of WFS1 protein within the intraluminal compartment. Furthermore, as shown in Fig. 3C, although endoglycosidase H (Endo H) treatment of the wild-type WFS1 protein resulted in faster migration of the protein, the mobility of the double mutant [WFS1 (N663D/N748D)] protein was not affected by treatment with Endo H. In addition, the double mutant protein exhibited the same mobility as the wild-type WFS1 protein treated with Endo H. These data demonstrated that no asparagine residue other than N663 and N748 is glycosylated.

Reduced protein stability of N-glycosylation-defective WFS1 protein

N-glycosylation reportedly plays an important role in the stability of proteins such as the T cell antigen receptor α-subunit [16], the α-subunit of the nicotinic acetylcholine receptor [17], and apolipoprotein B [18]. Therefore, to assess the role of N-glycosylation in WFS1 protein stability, we performed pulse-chase

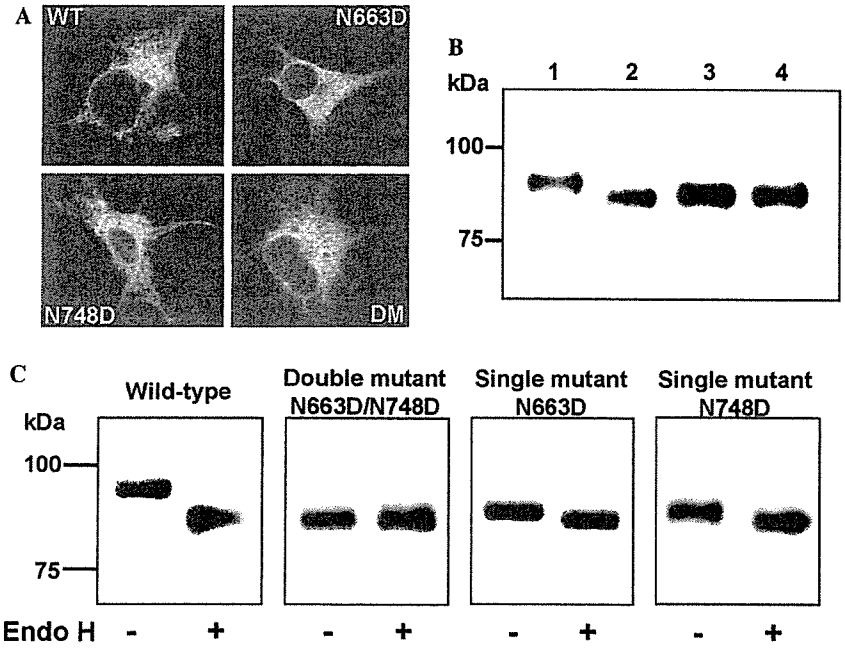

Fig. 3. Electrophoretic mobility and effect of endoglycosidase digestion on HA-tagged wild-type and mutant WFS1 proteins. (A) Immunofluorescence localization of HA-tagged WFS1 proteins: upper left, wild-type HA-mWFS1; upper right, HA-mWFS1(N663D); lower left, HA-mWFS1(N748D); lower right, HA-mWFS1(N663D/N748D). (B) COS7 cells transfected with 0.5 μg plasmids encoding either HA-tagged wild-type or mutant WFS1 proteins were lysed, subjected to SDS/PAGE, and probed with anti-HA antibody: lane 1, HA-mWFS1; lane 2, HA-mWFS1 (N663D/N748D); lane 3, HA-mWFS1(N663D); and lane 4, HA-mWFS1(N748D). (C) Lysates of COS7 cells transfected with either wild-type WFS1 cDNA or mutant constructs were incubated at 37 °C for 1 h with or without endoglycosidase H (500 U) and were subjected to electrophoresis on NuPAGE 3–8% Tris–acetate gel.

experiments. In these experiments, COS7 cells transiently transfected with either the HA-wild-type mWFS1 or mutant HA-mWFS1(N663D/N748D) cDNAs were labeled for 3 h with [^{35}S]methionine/cysteine and chased for different intervals. As shown in Fig. 4, the wild-type mWFS1 protein was relatively stable; 65 ± 6% ($n = 3$) of the protein remained 18 h after its synthesis. In contrast, only 44 ± 5% ($n = 3$) of mWFS1(N663D/N748D) remained after 18 h. These data showed protein stability to be reduced when both N-glycosylation sites were disrupted. One could argue an increased turnover rate of mWFS1(N663D/N748D) to be due to introducing aspartate residues rather than lack of glycosylation. To study the roles of N-glycosylation in various glycoproteins, asparagine residues in the consensus motif have been substituted with a variety of amino acids, such as aspartate ([19,20], this study), glutamine [14,21], alanine [19,22], threonine [23], and isoleucine [24]. None of these replacements were perfect, because introducing different residues might have its own effects. In this study, we also observed that WFS1 protein in MIN6 cells was more rapidly degraded when treated with a glycosylation inhibitor, tunicamycin (Fig. 1E). Thus, both molecular and biochemical approaches indicated that glycosylation-defective WFS1 protein has reduced stability. We therefore conclude that N-glycosylation affects WFS1 protein levels. A previous study using the ER resident glycoprotein ribophorin showed N-glycosylation to be necessary for calnexin binding, which prevents the glycoprotein from being rapidly degraded [25]. Such a mechanism could also be operative in WFS1 protein.

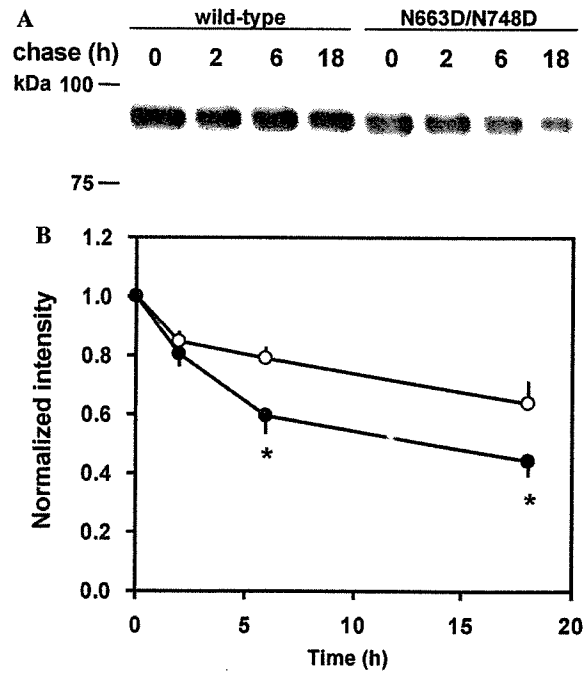

Fig. 4. Decreased stability of glycosylation-defective WFS1 protein. (A) HA-mWFS1 and HA-mWFS1(N663D/N748D) profiles of radiolabeled bands as a function of time of chase. A representative result from three experiments is shown. (B) Data from three experiments are summarized after normalization to time zero of chase. *$P < 0.05$.

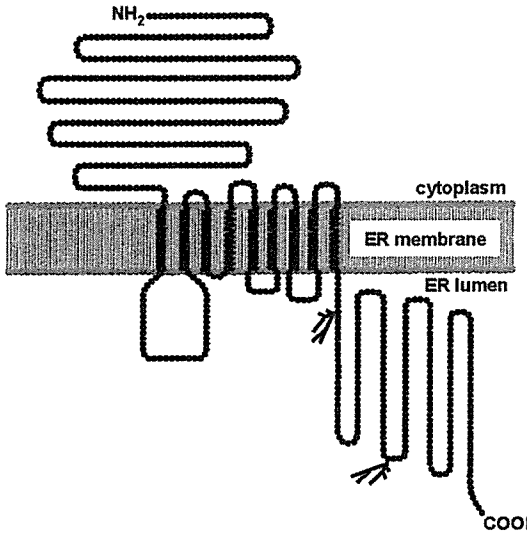

Fig. 5. Transmembrane topology model for mouse WFS1 protein with glycosylation sites. Membrane topology of mouse WFS1 protein as based on analysis using the SOSUI computer program [26] and data obtained in this study. Two N-glycosylation sites in the C-terminus stretch are depicted.

Herein, we defined the membrane topology of WFS1 by analyzing protease protection susceptibility: the orientation of the N-terminus in the cytoplasm and the C-terminus in the ER. This topology was supported by determining the N-glycosylation sites to be N663 and N748. A schematic diagram of WFS1 protein deduced from the current study and others is shown in Fig. 5. WFS1 protein/wolframin is a type II transmembrane protein and has long N-terminal and C-terminal stretches. These stretches could interact with other molecule(s), thereby mediating specific functions. Further study of these actions is clearly warranted. N663 and N748 residues in murine WFS1 protein correspond to N661 and N746 in the human orthologue. Although more than 100 mutations have been identified in WFS1 protein/wolframin and span the entire coding sequence, no mutations in these asparagine residues or adjacent amino acids were found in patients with Wolfram syndrome or LFSNHL. Given that loss of the functions of this protein is at least one of the pathogenic mechanisms of Wolfram syndrome [6,15], future survey of genomic sequences in patients with these diseases might identify mutations in these glycosylation sites.

The present data also provide evidence that increased WFS1 expression is the primary response of this protein to ER stress. There is no increase in WFS1 protein expression in response to tunicamycin, despite increased WFS1 mRNA levels. This is apparently attributable to the combined effects of increased mRNA levels and reduced protein stability. The increased WFS1 expression in response to ER-stress raises the possibility that WFS1 protein is a component of the UPR and plays a protective role against ER stress. This notion is supported by our recent findings that islets isolated from WFS1-deficient mice exhibited increased susceptibility to ER stress-induced apoptosis [7].

Acknowledgments

We are grateful to Y. Nagura for her expert technical assistance. This work was supported by a grant from Suzuken Memorial Foundation to H.I. and a Grant-in-Aid for Scientific Research (13204062) to Y.O. from the Ministry of Education, Science, Sports and Culture of Japan.

References

[1] K. Takeda, H. Inoue, Y. Tanizawa, Y. Matsuzaki, J. Oba, Y. Watanabe, K. Shinoda, Y. Oka, WFS1 (Wolfram syndrome 1) gene product: predominant subcellular localization to endoplasmic reticulum in cultured cells and neuronal expression in rat brain, Hum. Mol. Genet. 10 (2001) 477–484.

[2] H. Inoue, Y. Tanizawa, J. Wasson, P. Behn, K. Kalidas, E. Bernal-Mizrachi, M. Mueckler, H. Marshall, H. Donis-Keller, P. Crock, D. Rogers, M. Mikuni, H. Kimashiro, K. Higashi, G. Sobue, Y. Oka, M.A. Permutt, A gene encoding a transmembrane protein is mutated in patients with diabetes mellitus and optic atrophy (Wolfram syndrome), Nat. Genet. 20 (1998) 143–148.

[3] T.M. Strom, K. Hoetnagael, S. Hofmann, F. Gekeler, C. Scharfe, W. Rabl, K.D. Gerbitz, T. Meitinger, Diabetes insipidus, diabetes mellitus, optic atrophy and deafness (DIDMOAD) caused by mutations in a novel gene (wolframin) coding for a predicted transmembrane protein, Hum. Mol. Genet. 7 (1998) 2021–2028.

[4] I.N. Bespalova, G. Van Camp, S.J. Bom, D.J. Brown, K. Cryns, A.T. DeWan, A.E. Erson, K. Flothmann, H.P. Kunst, P. Kurnool, T.A. Sivakumaran, W.W.R.J. Cremers, S.M. Leal, M. Burmeister, M.M. Lesperance, Mutations in the Wolfram syndrome 1 gene (*WFS1*) are a common cause of low frequency sensorineural hearing loss, Hum. Mol. Genet. 15 (2001) 2501–2508.

[5] T.L. Young, E. Ives, E. Lynch, R. Person, S. Snook, L. MacLaren, T. Cater, A. Griffin, B. Fernandez, M.K. Lee, M.-C. King, Non-syndromic progressive hearing loss DFNA38 is caused by heterozygous missense mutation in the Wolfram syndrome gene WFS1, Hum. Mol. Genet. 15 (2001) 2509–2514.

[6] K. Cryns, T.A. Sivakumaran, J.M. Van den Ouweland, R.J. Pennings, C.W. Cremers, K. Flothmann, T.L. Young, R.J. Smith, M.M. Lesperance, G. Van Camp, Mutational spectrum of the WFS1 gene in Wolfram syndrome, nonsyndromic hearing impairment, diabetes mellitus, and psychiatric disease, Hum. Mutat. 22 (2003) 275–287.

[7] H. Ishihara, S. Takeda, A. Tamura, R. Takahashi, S. Yamaguchi, D. Takei, T. Yamada, H. Inoue, H. Soga, H. Katagiri, Y. Tanizawa, Y. Oka, Disruption of the WFS1 gene in mice causes progressive beta-cell loss and impaired stimulus-secretion coupling in insulin secretion, Hum. Mol. Genet. 13 (2004) 1159–1170.

[8] R. Kaufmann, Orchestrating the unfolded protein response in health and disease, J. Clin. Invest. 110 (2002) 1389–1398.

[9] H.P. Harding, D. Ron, Endoplasmic reticulum stress and the development of diabetes, Diabetes 51 (Suppl. 3) (2002) S455–S461.

[10] A.A. Osman, M. Saito, C. Makepeace, M.A. Permutt, P. Schlesinger, M. Mueckler, Wolframin expression induces novel ion channel activity in endoplasmic reticulum membranes and increases intracellular calcium, J. Biol. Chem. 278 (2003) 52755–52762.

[11] K. Cryns, S. Thys, L. van Laer, Y. Oka, M. Pfister, L. van Nassauw, R.J.H. Smith, J.P. Timmermans, G. Van Camp, The WFS1 gene, responsible for low frequent sensorineural hearing loss and Wolfram syndrome, is expressed in a variety of inner ear cells, Histochem. Cell Biol. 119 (2003) 247–256.
[12] H. Ishihara, T. Asano, K. Tsukuda, H. Katagiri, K. Inukai, M. Anai, M. Kikuchi, Y. Yazaki, J.I. Miyazaki, Y. Oka, Pancreatic beta cell line MIN6 exhibits characteristics of glucose metabolism and glucose-stimulated insulin secretion similar to those of normal islets, Diabetologia 36 (1993) 1139–1145.
[13] K.F. Ferri, G. Koemer, Organelle-specific initiation of cell death pathways, Nat. Cell Biol. 3 (2001) E255–E263.
[14] T. Michikawa, H. Hamanaka, H. Otsu, A. Yamamoto, A. Miyawaki, T. Furuichi, Y. Tashiro, K. Mikoshiba, Transmembrane topology and sites of N-glycosylation of inositol 1,4,5-trisphosphate receptor, J. Biol. Chem. 269 (1994) 9184–9189.
[15] S. Hofmann, C. Philbrook, K.D. Gerbitz, M.F. Bauer, Wolfram syndrome: structural and functional analyses of mutant and wild-type wolframin, the WFS1 gene product, Hum. Mol. Genet. 12 (2003) 2003–2012.
[16] K.P. Kearse, D.B. Williams, A. Singer, Persistence of glucose residues on core oligosaccharides prevents association of TCR alpha and TCR beta proteins with calnexin and results specifically in accelerated degradation of nascent TCR alpha proteins within the endoplasmic reticulum, EMBO J. 273 (1994) 17064–17072.
[17] S.H. Keller, J. Lindstrom, P. Taylor, Inhibition of glucose trimming with castanospermine reduces calnexin association and proteosome degradation of the alpha-subunit of the nicotinic acetylcholine receptor, J. Biol. Chem. 273 (1998) 17064–17072.
[18] Y. Chen, F. Caherec, S.L. Chuck, Calnexin and other factors that alter translocation affects the rapid binding of ubiquitin to apoB in the Sec61 complex, J. Biol. Chem. 273 (1998) 11887–11894.
[19] T.K. Lee, A.S. Koh, Z. Cui, R.H. Pierce, N. Ballatori, N-glycosylation controls functional activity of Oatp1, an organic anion transporter, Am. J. Physiol. Gastrointest. Liver Physiol. 285 (2003) G371–G381.
[20] L. Niu, M.L. Heaney, J.C. Vera, D.W. Golde, High-affinity binding to the GM-CSF receptor requires intact N-glycosylation sites in the extracellular domain of the β subunit, Blood 95 (2000) 3357–3362.
[21] Q. Gong, C.L. Anderson, C.T. January, Z. Zhou, Role of glycosylation in cell surface expression and stability of HERG potassium channels, Am. J. Physiol. Heart Circ. Physiol. 283 (2002) H77–H84.
[22] J. He, A.M. Castleberry, A.G. Lau, R.A. Hall, Glycosylation of β_1-adrenergic receptors regulates receptor surface expression and dimerization, Biochem. Biophys. Res. Commun. 297 (2002) 565–572.
[23] N. Buhlmamm, A. Aldecoa, K. Leuthauser, R. Gujer, R. Muff, J.A. Fischer, W. Born, Glycosylation of the calcitonin receptor-like receptor at Asn(60) or Asn(112) is important for cell surface expression, FEBS Lett. 486 (2000) 320–324.
[24] M. Ramanujam, J. Hofmann, H.L. Nakhasi, C.D. Atreya, Effect of site-directed asparagine to isoleucine substitutions at the N-linked E1 glycosylation sites on rubella virus viability, Virus Res. 81 (2001) 151–156.
[25] M. de Virgilio, C. Kitzmueller, E. Schwaiger, M. Klein, G. Kreibich, N.E. Ivessa, Degradation of a short-lived glycoprotein from the lumen of the endoplasmic reticulum: the role of N-inked glycans and the unfolded protein response, Mol. Biol. Cell 10 (1999) 4059–4073.
[26] T. Hirokawa, S. Boon-Chieng, S. Mitaku, SOSUI: classification and secondary structure prediction system for membrane proteins, Bioinformatics 14 (1998) 378–379.

Diabetologia (2004) 47:794–805
DOI 10.1007/s00125-004-1391-x

Diabetologia

Oxidative stress induces insulin resistance by activating the nuclear factor-κB pathway and disrupting normal subcellular distribution of phosphatidylinositol 3-kinase

T. Ogihara[1,2] · T. Asano[1] · H. Katagiri[2] · H. Sakoda[3] · M. Anai[3] · N. Shojima[1] · H. Ono[3] · M. Fujishiro[1] · A. Kushiyama[1] · Y. Fukushima[1] · M. Kikuchi[3] · N. Noguchi[4] · H. Aburatani[4] · Y. Gotoh[5] · I. Komuro[6] · T. Fujita[1]

[1] Department of Internal Medicine, Graduate School of Medicine, University of Tokyo, Tokyo, Japan
[2] Division of Advanced Therapeutics for Metabolic Diseases, Center for Translational and Advanced Animal Research on Human Diseases, Tohoku University Graduate School of Medicine, Sendai, Japan
[3] The Institute for Adult Diseases, Asahi Life Foundation, Tokyo, Japan
[4] Research Center for Advanced Science and Technology, University of Tokyo, Tokyo, Japan
[5] Department of Molecular Biology, Institute of Molecular and Cellular Biosciences, University of Tokyo, Tokyo, Japan
[6] Department of Cardiovascular Science and Medicine, Chiba University Graduate School of Medicine, Chiba, Japan

Abstract

Aims/hypothesis. Oxidative stress is associated with diabetes, hypertension and atherosclerosis. Insulin resistance is implicated in the development of these disorders. We tested the hypothesis that oxidative stress induces insulin resistance in rats, and endeavoured to identify mechanisms linking the two.
Methods. Buthionine sulfoximine (BSO), an inhibitor of glutathione synthase, was administered to Sprague-Dawley rats and 3T3-L1 adipocytes. Glucose metabolism and insulin signalling both in vivo and in 3T3-L1 adipocytes were examined. In 3T3-L1 adipocytes, the effects of overexpression of a dominant negative mutant of inhibitory κB (IκB), one role of which is to block oxidative-stress-induced nuclear factor (NF)-κB activation, were investigated.
Results. In rats given BSO for 2 weeks, the plasma lipid hydroperoxide level doubled, indicating increased oxidative stress. A hyperinsulinaemic-euglycaemic clamp study and a glucose transport assay using isolated muscle and adipocytes revealed insulin resistance in BSO-treated rats. BSO treatment also impaired insulin-induced glucose uptake and GLUT4 translocation in 3T3-L1 adipocytes. In BSO-treated rat muscle, adipose tissue and 3T3-L1 adipocytes, insulin-induced IRS-1 phosphorylation in the low-density microsome (LDM) fraction was specifically decreased, while that in whole cell lysates was not altered, and subsequent translocation of phosphatidylinositol (PI) 3-kinase from the cytosol and the LDM fraction was disrupted. BSO-induced impairments of insulin action and insulin signalling were reversed by overexpressing the dominant negative mutant of IκB, thereby suppressing NF-κB activation.
Conclusions/interpretation. Oxidative stress induces insulin resistance by impairing IRS-1 phosphorylation and PI 3-kinase activation in the LDM fraction, and NF-κB activation is likely to be involved in this process.

Keywords Buthionine sulfoximine · Glutathione · Hyperinsulinaemic-euglycaemic clamp · Inhibitory κB · Insulin resistance · IRS · Nuclear factor-κB · Oxidative stress · Phosphatidylinositol 3-kinase

Received: 20 October 2003 / Accepted: 26 January 2004
Published online: 1 May 2004

T. Asano (✉)
Department of Internal Medicine, Graduate School of Medicine, University of Tokyo, Tokyo 113-8655, Japan
E-mail: asano-tky@umin.ac.jp
Tel.: +81-3-38153411 ext. 33133, Fax: +81-3-58031874

Present address:
T. Asano
Department of Physiological Chemistry and Metabolism, Graduate School of Medicine, University of Tokyo, Tokyo 113-8655, Japan

Introduction

Oxidative stress represents an imbalance between production of reactive oxygen species and the antioxidant defence system [1]. Oxidative stress is widely recognised as being associated with various disorders including diabetes, hypertension and atherosclerosis. In-

Abbreviations: BSO, buthionine sulfoximine · GMSA, gel mobility shift assay · IκB, inhibitory κB · IKK, IκB kinase · LDM, low-density microsome · NF-κB, nuclear factor-κB · PI, phosphatidylinositol

sulin resistance is a common feature of these disorders [2, 3]. Indeed, in diabetic people and in animal models of diabetes, the plasma free radical concentration is increased [4, 5] and antioxidant defences are diminished [6, 7]. It has also been suggested that antioxidant agents such as vitamin C [8] and E [9] improve insulin action in diabetic subjects.

Angiotensin II reportedly induces free radical production and increases plasma oxidative stress [10]. In our previous study, we showed continuous infusion of angiotensin II to induce insulin resistance with increased oxidative stress in rats, while the spin trap agent tempol [11], which works as a superoxide dismutase mimetic, decreases oxidative stress and improves insulin resistance in these rats [12]. A similar coexistence of oxidative stress and insulin resistance, as well as recovery with tempol administration was observed in adrenomedullin-deficient mice [13]. These previous reports strongly suggest a close relationship between oxidative stress and insulin resistance. Thus, we attempted to elucidate the molecular mechanisms underlying insulin resistance and oxidative stress.

In this study, to increase oxidative stress in vivo, we utilised a selective inhibitor of γ-glutamylcysteine synthetase, i.e. an inhibitor of glutathione synthase, buthionine sulfoximine (BSO). Glutathione is one of the major components of the antioxidant defence system, such that BSO administration increases oxidative stress by reducing the tissue glutathione level [14]. Although BSO does not have toxic effects in animals [14], BSO-treated rats were previously shown to exhibit glucose intolerance [15] and hypertension [16]. In the current study, we examined the effect of BSO treatment on insulin resistance in rats and 3T3-L1 adipocytes. We investigated the molecular mechanisms underlying BSO-induced insulin resistance, focusing on the subcellular distribution of phosphatidylinositol (PI) 3-kinase. Finally, we examined the involvement of the nuclear factor (NF)-κB pathway in BSO-induced insulin resistance and insulin signalling impairment.

Materials and methods

Materials. Affinity-purified antibodies against IRS-1 and GLUT4 were prepared as previously described [17]. Antibodies against phosphotyrosine, the p85 subunit of PI 3-kinase, and inhibitory κB (IκB) were purchased from Upstate Biotechnology (Milton Keynes, UK). TNF-α and buthionine-[S, R]-sulfoximine (BSO) were purchased from Sigma-Aldrich (St. Louis, Mo., USA).

Animals. Seven-week-old male Sprague-Dawley rats (Tokyo Experimental Animals, Tokyo, Japan) were fed a standard rodent diet with or without water containing 30 mmol/l BSO for 14 days [16]. The animal care was in accordance with the policies of the University of Tokyo, and the "Principles of laboratory animal care" (NIH publication no. 85-23, revised 1985) were followed.

Measurements. Cholesteryl ester hydroperoxides were analysed by HPLC, with 234 nm UV detection and post-column chemiluminescence detection on an LC-8 column (Supelco, 4×250 mm, 5-μm particles; Sigma-Aldrich) and methanol/tert-butyl alcohol (95/5 vol) as the eluent, as reported previously but with slight modification [18]. In brief, plasma was extracted with 10 volumes of methanol and 50 volumes of hexane. The hexane phase was removed, dried under N_2 gas and redissolved in an eluent for HPLC injection. Liver glutathione content was measured spectrophotometrically using a glutathione reductase recycling assay, as described previously [19].

Hyperinsulinaemic-euglycaemic clamp study. Rats fasted overnight were anaesthetised by intraperitoneal injection of pentobarbital sodium (60 mg/kg body weight) and the left jugular and femoral veins were catheterised for blood sampling and infusion respectively. Hyperinsulinaemic-euglycaemic clamp analysis was performed as described previously [17]. The glucose utilisation rate, hepatic glucose production and an estimate of muscle glucose uptake during the clamp (defined as the glucose metabolic index) were calculated as previously described [20].

Glucose uptake into isolated soleus muscle. Rats fasted overnight were anaesthetised and soleus muscles were dissected out and rapidly cut into 20–40 mg strips. The rats were then killed by intracardiac injection of pentobarbital. Isolated soleus muscle was incubated for 20 min with or without 1.44×10^{-8} mol/l human insulin (this concentration is equivalent to 2 mU/ml), as described previously [17]. 2-Deoxy glucose uptake into the isolated soleus muscle strips was measured using 2-deoxy-D-[^{3}H]glucose and [^{14}C]manitol as described previously [21].

Preparation of rat adipocytes and measurement of glucose uptake. Isolated rat adipocytes were prepared from epididymal adipose tissue harvested from fasted rats using the collagenase method [22], and 2-deoxy glucose uptake was then assayed as previously described [23].

Adenovirus-mediated gene transfer to 3T3-L1 adipocytes. 3T3-L1 fibroblasts were maintained in DMEM supplemented with 10% donor calf serum and differentiated into adipocytes as previously described [24]. The dominant negative mutant of IκB-α, in which serine residues 32 and 36 were substituted with alanine, was kindly provided by Dr R. Gaynor (University of Texas Southwestern Medical Center at Dallas, Tex., USA). To obtain recombinant adenovirus, pAdeno-X was ligated with cDNA encoding *Escherichia coli* lacZ and dominant negative IκB according to the manufacturer's instructions for the Adeno-X Expression System (Clontech, Palo Alto, Calif., USA). Infection of 3T3-L1 adipocytes with the adenovirus was carried out as described previously [25]. Recombinant adenoviruses were applied at a multiplicity of infection of approximately 200–300 pfu/cell and 3T3-L1 adipocytes infected with lacZ virus were used as a control.

Gel mobility shift assay. Nuclear protein extracts from 3T3-L1 adipocytes were prepared using NE-PER nuclear and cytoplasmic extraction reagents (Pierce Biotechnology, Rockford, Ill., USA) according to the manufacturer's instructions and used for gel mobility shift assay (GMSA). Briefly, 3T3-L1 adipocytes were homogenised in 1 ml of PBS and centrifuged for 10 min at 500 × *g* at 4 °C. After removing the supernatant, the pellet was resuspended in 500 μl of Cytoplasmic Extraction Reagent I buffer containing protease inhibitors (1 600 mol/l benzamidine, 0.3 mmol/l aprotinin, 4.2 mol/l leupeptin, 0.2 mol/l phenylmethylsulfonyl fluoride), and was incubated

on ice for 10 min. Then, 27.5 µl of Cytoplasmic Extraction Reagent II buffer were added to the sample, which was vortexed and centrifuged at 16 000 × *g* for 5 min. The resultant pellet was resuspended in 250 µl of NER buffer, vortexed every 10 minutes for 40 min and then centrifuged at 16 000 × *g* for 10 min. The supernatant containing nuclear proteins was stored at −80 °C. For the GMSA, 10 µg of nuclear proteins were incubated in binding buffer with 3.5 pmol of double-stranded DNA oligonucleotide containing an NF-κB consensus-binding sequence labelled with [^{32}P]-ATP using T4 polynucleotide kinase for 30 min at 37 °C. For supershift analyses, monoclonal antibody against NF-κB p65 was separately pre-incubated with nuclear extracts at 4 °C for 20 min in a total volume of 16 µl of binding buffer, followed by incubation with 8 µl of ^{32}P-labelled oligonucleotide probe with and without cold oligonucleotide probe at 4 °C for 20 min using a Nushift Kit (Geneka Biotechnology, Carlsbad, Calif., USA). Protein-DNA complexes were separated from the unbound DNA probe by electrophoresis through 5% polyacrylamide gels containing 1× Tris-glycine-EDTA buffer. The gel was dried and exposed to BAS2000 (Fujifilm, Tokyo, Japan).

Glucose uptake into 3T3-L1 adipocytes. 3T3-L1 adipocytes plated in 24-well culture dishes were serum starved for 3 h in DMEM containing 0.2% bovine serum albumin, after which they were incubated in Krebs–Ringer phosphate buffer for an additional 45 min, prior to incubation with or without 10^{-6} or 10^{-7} mol/l insulin for 15 min. The assay was initiated by adding 2-deoxy-D-[^{3}H]glucose (1.85×10^{7} Bq/sample, 0.1 mmol) and was terminated 4 min later by washing the cells once with ice-cold Krebs–Ringer phosphate buffer containing 0.3 mmol/l phloretin and then twice with ice-cold Krebs–Ringer phosphate buffer. The cells were then solubilised in 0.1% SDS, and the incorporated radioactivity was determined by scintillation counting [26].

Subcellular fractionation. 3T3-L1 adipocytes were serum starved for 3 h and incubated with or without 10^{-6} mol/l insulin for 15 min. Cells were fractionated as described previously [27]. Briefly, 3T3-L1 adipocytes were resuspended in HES buffer (255 mmol/l sucrose, 20 mmol/l HEPES [pH 7.4], 1 mmol/l EDTA), homogenised and subjected to differential centrifugation. The supernatants from the following spins were serially removed and pelleted in a Ti70 rotor as follows: 19 000 × *g* (20 min), 41 000 × *g* (20 min) and 180 000 × *g* (75 min). The first 19 000 × *g* pellet was resuspended, loaded onto a sucrose cushion (1.12 mol/l sucrose, 20 mmol/l HEPES [pH 7.4], 1 mmol/l EDTA) and isolated from the interface yielding the plasma membrane fraction as the pellet of a 41 000 × *g* spin (20 min). The last 180 000 × *g* pellet corresponded to the low-density microsome (LDM) fraction. Subcellular fractionation and measurement of GLUT4 translocation in isolated skeletal muscle and adipocytes from rats were described previously [12]. After resuspension of the pellets in solubilisation buffer, 20 µg of each fraction were loaded for western blotting. Proteins in the plasma membrane and LDM fractions were separated by SDS-PAGE, transferred to a polyvinylidene fluoride membrane, immunoblotted with anti-GLUT4, anti-IRS-1 or anti-p85 antibodies, and reacted with enhanced chemiluminescence reagent (Amersham Biosciences, Uppsala, Sweden) or subject to immunoprecipitation and PI 3-kinase assay of the immunoprecipitates as previously described [17].

Immunoprecipitation and immunoblotting. In rat experiments, rats fasted overnight were anaesthetised, and within 10–15 min the abdominal cavity was opened, the portal vein exposed, and 16 ml/kg body weight of normal saline (0.9% NaCl), with or without 10^{-5} mol/l human insulin, were injected. After 60 s, hindlimb muscles were removed and immediately homogenised as described previously [28]. In 3T3-L1 experiments, 3T3-L1 adipocytes were serum-starved for 18 h, pre-incubated with or without 80 µmol/l BSO for 18 h, then stimulated with or without 10^{-6} mol/l insulin for 15 min. The cells were then washed and lysed with lysis buffer as described previously [29]. After centrifugation, the resultant supernatants were used for immunoprecipitation or immunoblotting as described previously [28]. Proteins were visualised with enhanced chemiluminescence and band intensities were quantified with a Molecular Imager GS-525 using Imaging Screen-CH (Bio-Rad Laboratories, Hercules, Calif., USA). In some experiments, 3T3-L1 cells were incubated with 5.8 pmol/l (equivalent to 10 ng/dl) TNF-α or 80 µmol/l BSO for 18 h, lysed and immunoblotted with anti-IκB antibody.

Phosphatidylinositol 3-kinase activity. After preparing tissue samples as above, IRS-1 was immunoprecipitated, and PI 3-kinase activity in the immunoprecipitates was assayed as previously described [17].

Statistical analysis. Data are expressed as means ± SE. Comparisons between the two groups were made using unpaired *t* tests. We considered *p* values of less than 0.05 to be statistically significant.

Results

Characterisation of rats studied. Although food intakes were similar in the two groups, the BSO-treated rats had lower body weights than control rats (Table 1). Individual water consumptions did not differ between the two. Systolic and diastolic blood pressures were similar in the two groups of rats. Fasting blood glucose and plasma insulin levels in BSO rats were also similar to those of control rats. Although fasting insulin levels were not elevated in BSO-treated rats as compared with those of controls, we found that

Table 1. Characterisation of BSO-treated rats

	Control	BSO
Body weight (g)	320.0±8.7	284±4.1*
Food intake (g/day)	20.2±2.4	21.2±2.3
Water intake (ml/day)	38.2±1.8	36.8±3.2
Systolic BP (mm Hg)	113.5±4.4	120.7±3.9
Diastolic BP (mm Hg)	83.4±4.4	87.8±1.4
Fasting blood glucose (mmol/l)	6.12±0.32	6.32±0.24
Randomly fed blood glucose (mmol/l)	8.37±0.24	8.44±0.17
Fasting plasma insulin (pmol/l)	109±16	112±3
Randomly fed plasma insulin (pmol/l)	188±17	367±3*
Glutathione content of liver (µmol/g tissue)	3.2±0.3	1.1±0.4*
Plasma cholesteryl ester hydroperoxide (mmol/l)	1.38±0.3	2.72±0.3*

Data are means ± SE; rats in each group, n=6; * p<0.05 compared with controls

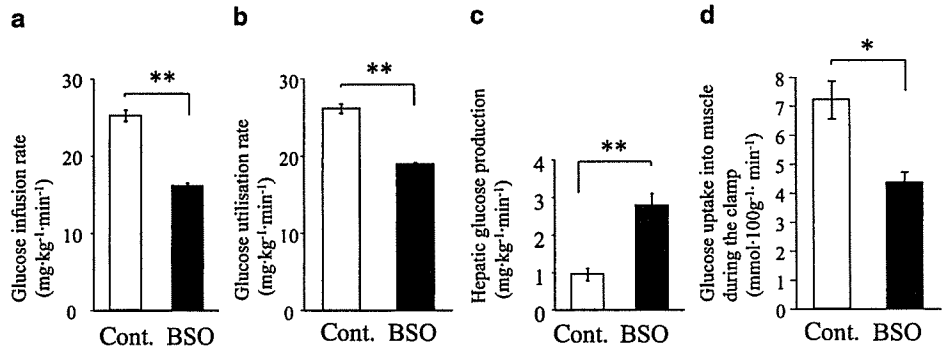

Fig. 1. A hyperinsulinaemic-euglycaemic clamp study. Rats were anaesthetised by intraperitoneal injection of pentobarbital sodium and the left jugular and femoral veins were catheterised for blood sampling and infusion respectively. Hyperinsulinaemic-euglycaemic clamp analysis was performed as described previously [17]. The glucose infusion rate (**a**), glucose utilisation rate (**b**), hepatic glucose production (**c**) and muscle glucose uptake during the clamp (defined as the glucose metabolic index; **d**) were estimated from hyperinsulinaemic-euglycaemic clamp data. * $p<0.05$, ** $p<0.01$ compared with the control. Bars represent the means ± SE of results from four to five rats. Cont. indicates control Sprague-Dawley rats. BSO indicates rats fed a standard rodent diet with water containing 30 mmol/l BSO for 12 days

among well-fed animals, insulin levels in BSO-treated rats were significantly higher than those in controls. To determine the effect of BSO as a glutathione synthase inhibitor, hepatic glutathione content was measured, because glutathione is most abundant in the liver. The glutathione level was significantly lower, by 34%, in the livers of BSO-treated rats than in those of controls. The cholesteryl ester hydroperoxide level in BSO-treated rat plasma was double that in control rats, suggesting that oxidative stress is increased in BSO-treated rats.

Hyperinsulinaemic-euglycaemic clamp study. Whole-body insulin sensitivity was evaluated using a hyperinsulinaemic-euglycaemic clamp technique. Compared with controls, the glucose infusion rate was decreased by 36.2% and the glucose utilisation rate by 27.6% during submaximal insulin infusion in BSO-treated rats (Figs. 1a, b). In addition, hepatic glucose production was increased by 29.3% in BSO-treated rats, suggesting impairment of the ability of insulin to suppress hepatic glucose production (Fig. 1c). Glucose uptake into skeletal muscle during the clamp was decreased by 39.4% in BSO-treated rats (Fig. 1d). These results suggest that BSO treatment induces insulin resistance both systemically and in skeletal muscle and liver.

Insulin-induced glucose uptake and GLUT4 translocation in BSO-treated rat skeletal muscle and adipocytes. In BSO-treated rats, insulin-induced glucose uptakes into isolated soleus muscle and adipocytes were reduced by 21.4% and 47.8% respectively as compared with the control levels (Figs. 2a, c). Subsequent western blot analysis showed the GLUT4 contents of skeletal muscle and adipocytes to be similar in the two groups (Figs. 2b, d, upper panels), indicating that the impairment of insulin-induced glucose uptake in these tissues from BSO-treated rats was not due to reduced expression of GLUT4 proteins. However, insulin-induced GLUT4 translocation, as assessed by the appearance of GLUT4 in the plasma membrane fraction of skeletal muscle and adipose tissue, was decreased in BSO-treated rats (Figs. 2b, d, lower panels). Microscopic analysis revealed adipocytes from BSO-treated rats to be small, which is consistent with the low body weights of these rats (Fig. 2e), suggesting that insulin resistance in BSO-treated rats is not attributable to adipocyte enlargement.

Impairment of insulin signalling in BSO-treated rat skeletal muscle and adipocytes. Next, we investigated insulin-induced tyrosine phosphorylation of IRS-1, association of PI 3-kinase with IRS-1, and PI 3-kinase activation in skeletal muscle and adipose tissue in vivo by injecting insulin through the portal vein of anaesthetised rats. Protein amount and insulin-induced tyrosine phosphorylation of IRS-1 in skeletal muscle (whole tissue lysates) from BSO-treated rats were similar to those in controls (Fig. 3a, upper panels). Because the insulin signalling in the LDM fraction has been implicated in several insulin actions including insulin-induced glucose uptake [30, 31], we carried out subcellular fractionation studies of skeletal muscles from these rats. Subcellular fractionation data showed insulin-induced tyrosine phosphorylation of IRS-1 in the LDM fraction to be significantly decreased in BSO-treated rats as compared with controls, although the IRS-1 protein amount in this fraction was unchanged (Fig. 3a, upper panels). In the cytosol, the amount of IRS-1 and insulin-induced phosphorylation were similar in BSO-treated and control rat muscles (Fig. 3a, upper panels). Next, we investigated the amount of the p85 subunit for PI 3-kinase protein in whole tissue lysates, the LDM fraction and the cytosol (Fig. 3a, middle panels). The amounts of p85 protein were similar in whole tissue

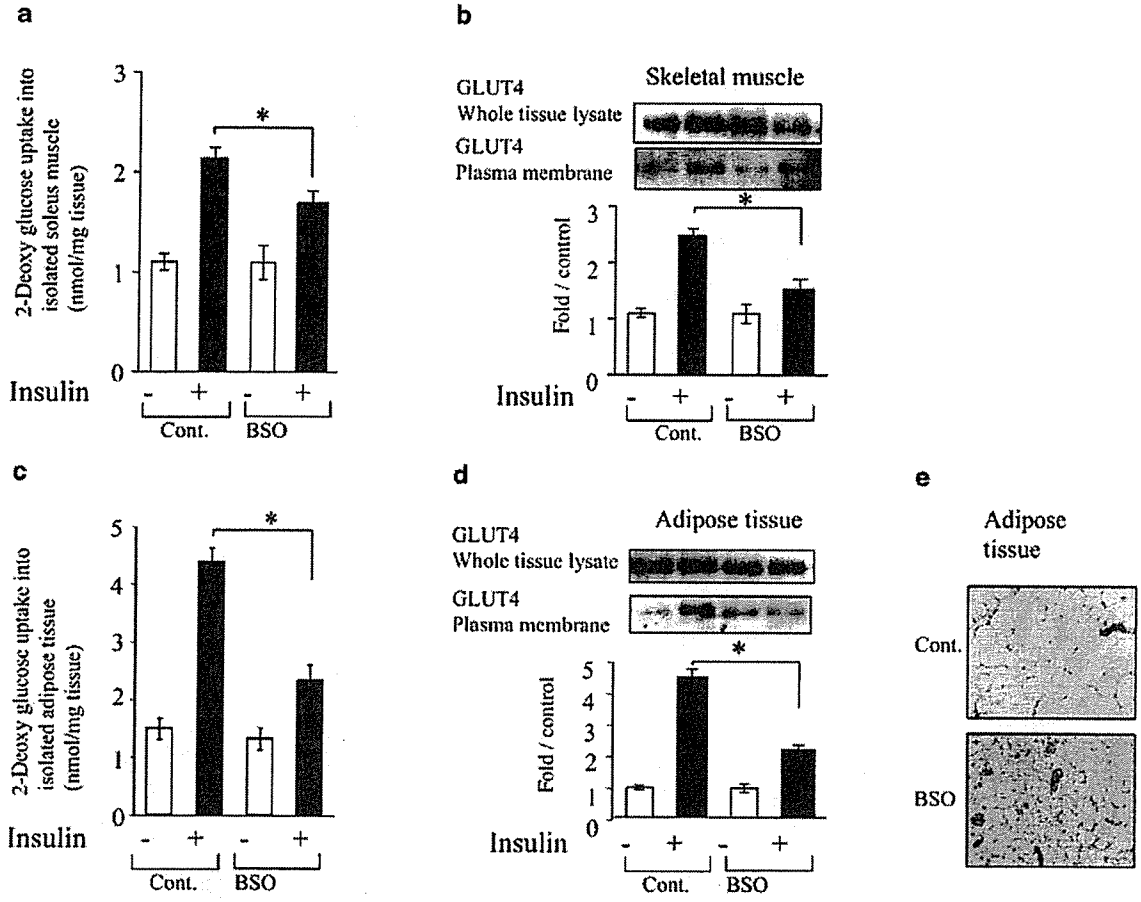

Fig. 2. Insulin resistance in isolated skeletal muscle and adipose tissue in BSO-treated rats. **a.** 2-Deoxy-glucose uptakes into isolated soleus muscle and adipose tissue (**c**). Isolated rat soleus muscle was incubated for 20 min with or without 1.44×10^{-8} mol/l human insulin (this concentration is equivalent to 2 mU/ml) as described previously [17]. 2-Deoxy-D-[1-^{3}H]glucose uptake into the isolated soleus muscle strips was measured as described previously [21]. Isolated rat adipocytes were prepared from epididymal adipose tissue harvested from fasted rats using the collagenase method [22], and 2-deoxy glucose uptake was then assayed as previously described [23]. **b, d.** GLUT4 protein amount in whole tissue lysates (upper panels), the plasma membrane fraction (lower panels) of skeletal muscle (**b**) and adipose tissue (**d**) under basal or insulin-stimulated conditions. Subcellular fractionation and measurement of GLUT4 translocation of isolated skeletal muscle and adipocytes from rats were described previously [12]. Whole tissue lysates and plasma membrane fractions were subjected to SDS-PAGE followed by immunoblotting with anti-GLUT4 antibody. The data are representative of three independent experiments. Bars depict means ± SE of the results from four to six samples. * $p<0.05$ compared with the control under the insulin-stimulated conditions. **d.** Haematoxylin and eosin stained adipose tissues from control and BSO-treated rats are shown. Cont. indicates control Sprague-Dawley rats. BSO indicates rats fed a standard rodent diet with water containing 30 mmol/l BSO for 12 days

lysates before and after insulin stimulation. However, insulin stimulation induced a p85 increase in the LDM fraction and a decrease in the cytosol, suggesting that insulin stimulates p85 translocation from the cytosol to the LDM fraction. This insulin-induced translocation of p85 was disrupted in BSO-treated rats. Insulin-induced increases in IRS-1-associated p85 protein and PI 3-kinase activity did not differ significantly between whole tissue lysates and the cytosol in either BSO-treated or control rat muscle (Fig. 3a, lower panels). However, both were significantly decreased in the LDM fraction of BSO-treated rats as compared with the controls. We obtained essentially the same results in the adipose tissue of these rats (Fig. 3b). In addition, we confirmed that insulin-induced tyrosine phosphorylation of the insulin receptor and IRS-2, as well as Ser-473 phosphorylation of Akt, in the whole tissue lysates of skeletal muscle and adipose tissue does not differ between BSO-treated and control rats (data not shown). Thus, early insulin-signalling steps were shown to be impaired specifically in the LDM fraction, but not in whole tissue lysates of skeletal muscle and adipose tissue from BSO-treated rats.

Insulin action and insulin signalling in BSO-treated 3T3-L1 adipocytes. To further investigate the impaired step in BSO-induced insulin resistance, 3T3-L1

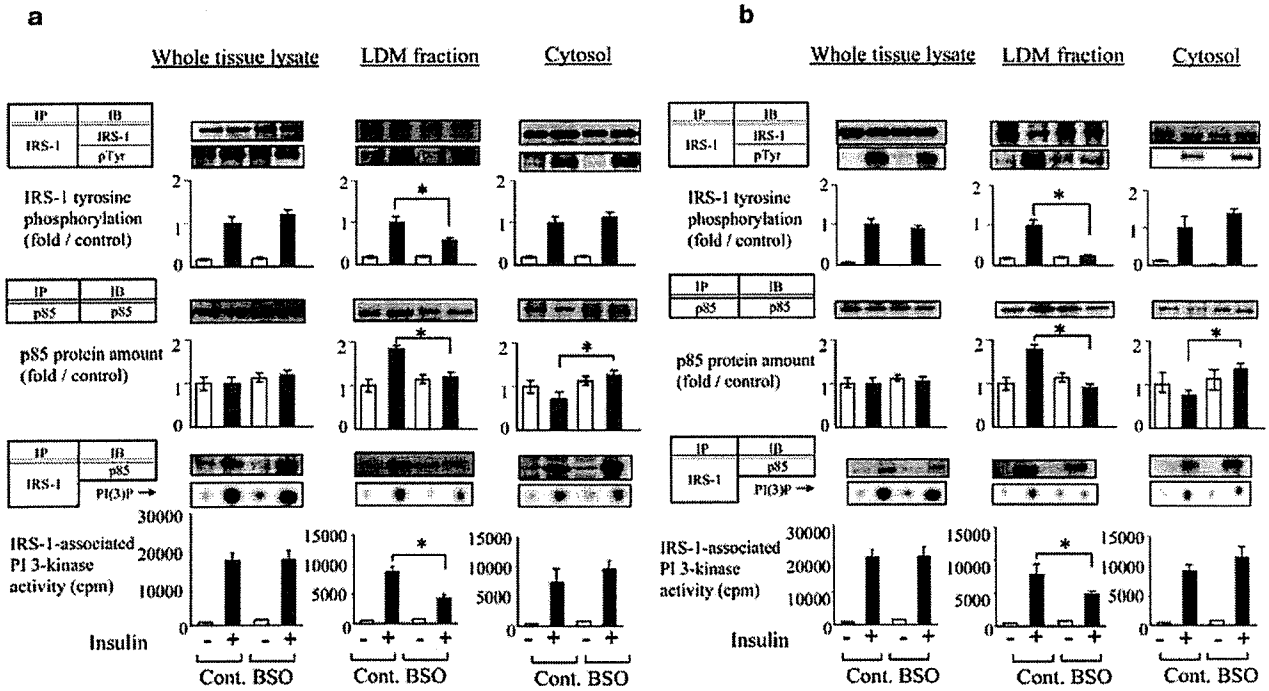

Fig. 3. Insulin signalling in skeletal muscle (**a**) and adipose tissue (**b**) from BSO-treated rats. Rats were anaesthetised, the portal vein exposed, and 16 ml/kg body weight of normal saline, with or without 10^{-5} mol/l human insulin, were injected. After 60 s, hindlimb muscles and epididymal fat were removed and immediately homogenised as described previously [28]. After centrifugation, the resultant supernatants were employed for immunoprecipitation or immunoblotting using the indicated antibodies as described previously [28]. Proteins were visualised with enhanced chemiluminescence and band intensities were quantified with a Molecular Imager GS-525 using Imaging Screen-CH (Bio-Rad). Bars depict means ± SE of the quantitated tyrosine phosphorylation bands, independently obtained in triplicate. Representative spots of PI(3)P are shown in the lower panels and bars depict means ± SE of PI 3-kinase activity measured in three independent assays. * $p<0.05$ compared with the control under the insulin-stimulated condition. IP, immunoprecipitation; IB, immunoblotting; pTyr, phosphotyrosine

adipocytes were incubated with 80 μmol/l BSO for 18 h [32]. It was reported that BSO treatment of adipocytes markedly decreases cellular glutathione levels and increases reactive oxygen species [15, 32]. Incubation with BSO did not affect the morphology or the viability of 3T3-L1 adipocytes (data not shown). Insulin-induced glucose uptake into 3T3-L1 adipocytes was decreased by 42.5% in BSO-treated cells (Fig. 4a). In these cells, insulin-induced GLUT4 translocation to the plasma membrane was impaired (Fig. 4b). Next, we determined insulin-induced IRS-1 phosphorylation and PI 3-kinase activation in whole cell lysates, the LDM fraction and the cytosol. As in rats, protein levels and insulin-induced tyrosine phosphorylations of IRS-1 and IRS-1-associated PI 3-kinase were unaffected by BSO treatment (Fig. 4c, upper panel). In control cells and in BSO-treated cells, p85 protein levels did not differ before versus after insulin stimulation. Next, we examined IRS-1 tyrosine phosphorylation and IRS-1 associated PI 3-kinase activity in the LDM fraction and the cytosol. While IRS-1 protein levels did not change after incubation with BSO, insulin-induced IRS-1 tyrosine phosphorylation in the LDM fraction was suppressed by BSO treatment (Fig. 4c, middle panel). The amount of p85 protein was increased in the LDM fraction and decreased in the cytosol after insulin stimulation, indicating that insulin induces p85 translocation from the cytosol to the LDM fraction in control cells. However, the p85 increase in the LDM fraction was clearly disrupted in BSO-treated cells (Fig. 4c, middle panel). In parallel, insulin-stimulation increased IRS-1-associated p85 protein levels and PI 3-kinase activity in the LDM fraction of control but not BSO-treated cells. Thus, BSO treatment disrupts insulin-induced IRS-1 phosphorylation in the LDM fraction and the subcellular redistribution of PI 3-kinase in 3T3-L1 adipocytes.

Inhibition of NF-κB activation improves BSO-induced insulin resistance. It is widely known that one potential target of oxidative stress is the activation of transcription factor NF-κB [33]. Oxidative stress and inflammatory cytokine stimulation reportedly activate upper kinase IκB kinase (IKK) which phosphorylates serine residues of IκB. The phosphorylated IκB is then subject to degradation, leading to translocation of NF-κB to the nucleus [34]. To investigate the role of NF-κB cascade activation in BSO-induced insulin re-

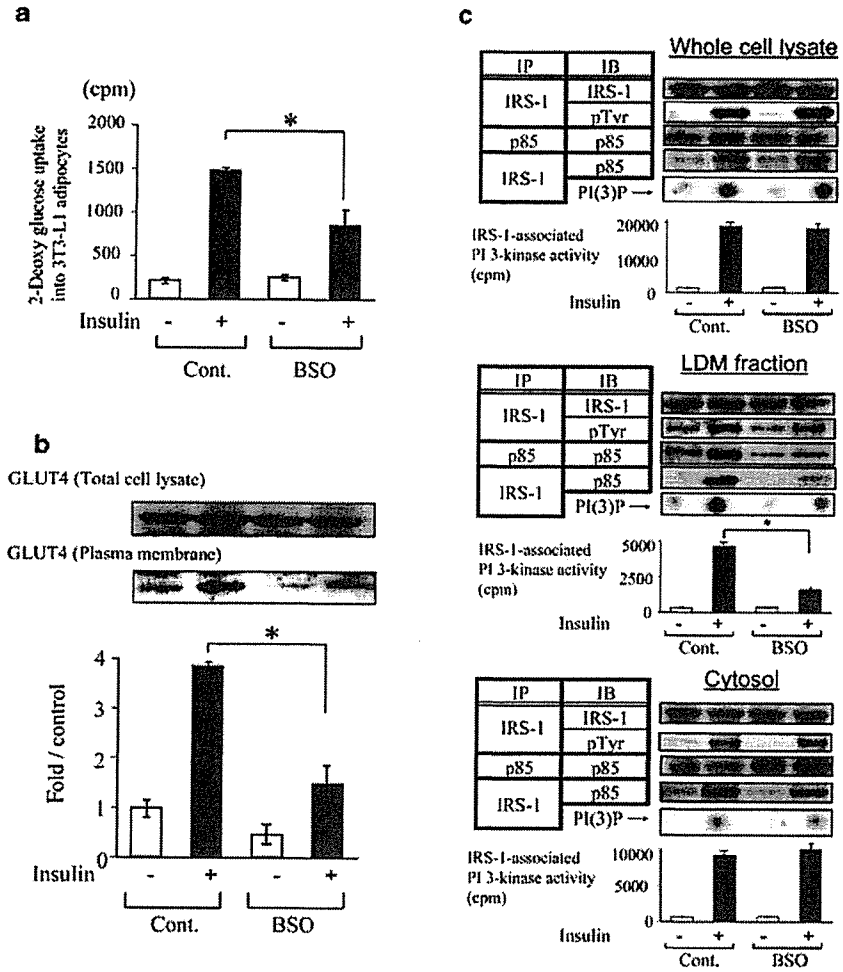

Fig. 4. Effects of BSO treatment on insulin action and insulin signalling in 3T3-L1 adipocytes. **a.** Insulin-induced 2-deoxy glucose uptake into 3T3-L1 adipocytes. 3T3-L1 adipocytes were serum-starved for 18 h, pre-incubated with or without 80 μmol/l BSO for 18 h, then incubated with or without 10^{-6} mol/l insulin for 15 min. 2-Deoxy glucose uptake was measured as described in Materials and methods. Bars depict means ± SE of results obtained independently in triplicate. * $p<0.05$ compared with the insulin-stimulated control. **b.** Recruitment of GLUT4 to the plasma membrane in 3T3-L1 adipocytes with or without BSO pretreatment. 3T3-L1 adipocytes were serum-starved for 18 h, pre-incubated with or without 80 μmol/l BSO for 18 h, then stimulated with or without 10^{-6} mol/l insulin for 15 min. Cells were fractionated as described previously [27]. The cell lysates and plasma membrane fraction were immunoblotted with anti-GLUT4 antibody. Representative immunoblots using anti-GLUT4 antibody are shown. Bars depict means ± SE of the quantitated bands of the plasma membrane fraction, independently obtained in triplicate. **c.** IRS-1 phosphorylation and IRS-1-associated PI 3-kinase in whole cell lysates (upper panels), the LDM fraction (middle panels) and the cytosol (lower panels) in 3T3-L1. 3T3-L1 adipocytes were serum-starved for 18 h, pre-incubated with or without 80 μmol/l BSO for 18 h, then stimulated with or without 10^{-6} mol/l insulin for 15 min. Subcellular fractionation was performed as described in Materials and methods. The whole cell lysates and fractions were used for immunoprecipitation, immunoblotting and PI 3-kinase assay as described previously [28]. Proteins were visualised with enhanced chemiluminescence and band intensities were quantified with a Molecular Imager GS-525. Representative immunoblots are shown in the upper and middle panels and representative spots of PI(3)P, independently obtained in triplicate, are shown in the lower panel. Bars depict means ± SE of the quantitated spots of PI(3)P, indicating IRS-1-associated PI 3-kinase activity, independently obtained in triplicate. Cont., control 3T3-L1 adipocytes; BSO, pre-treated with 80 μmol/l BSO for 18 h. * $p<0.05$ compared with the control under the insulin-stimulated condition

sistance, we overexpressed the dominant negative mutant of IκB in 3T3-L1 adipocytes using adenovirus. This mutant, characterised by the substitution of two serine phosphorylation sites to alanine, is resistant to degradation and inhibits NF-κB-induced transcription. In 3T3-L1 adipocytes, endogenous IκB was degraded by 5.8 pmol/l (equivalent to 10 ng/dl) of TNF-α or 80 μmol/l BSO pre-incubation for 18 h (Fig. 5a). However, the dominant negative IκB, overexpressed using adenovirus, was not degraded by these treat-

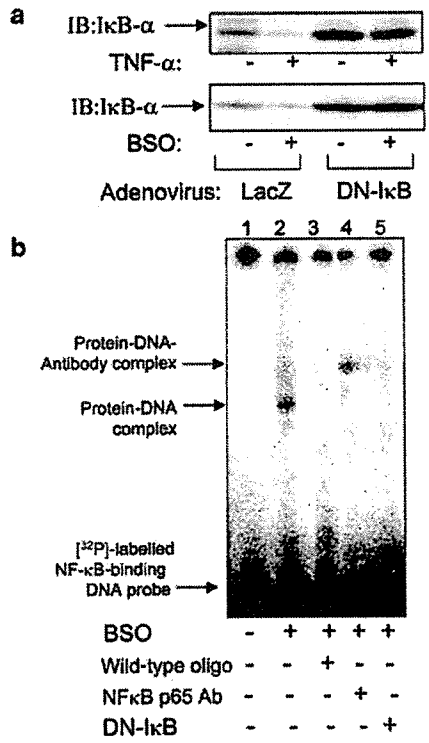

Fig. 5. Dominant negative mutant of IκB. **a.** Immunoblot of 3T3-L1 adipocytes overexpressing LacZ (control) and dominant negative mutant of I-κB adenoviruses. Representative immunoblots with anti-IκBα antibody of the cells incubated with 5.8 pmol/l (equivalent to 10 ng/ml) TNF-α and 80 μmol/l BSO for 18 h are shown in the upper and lower panels respectively. **b.** Gel mobility shift assay (GMSA). 3T3-L1 adipocytes were incubated with (lanes 2–5) or without (lane 1) 80 μmol/l BSO for 18 h. Dominant negative IκB was overexpressed in 3T3-L1 adipocytes (lane 5). Nuclear protein extracts from 3T3-L1 adipocytes were prepared as described in Materials and methods. For the GMSA, 10 μg of nuclear proteins were incubated in binding buffer with 3.5 pmol of double-stranded DNA oligonucleotide containing an NF-κB consensus binding sequence labelled with [^{32}P]-ATP using T4 polynucleotide kinase, for 30 min at 37 °C. For supershift analyses, monoclonal antibody against NF-κB p65 (NF-κB p65 Ab, lane 4) was separately pre-incubated with nuclear extracts at 4 °C for 20 min in a total volume of 16 μl of binding buffer, followed by incubation with 8 μl of ^{32}P-labelled oligonucleotide probe with and without a cold oligonucleotide probe (wild-type oligo, lane 3) at 4 °C for 20 min using a Nushift Kit (Geneka Biotechnology). Protein-DNA complexes were separated from the unbound DNA probe by electrophoresis through 5% polyacrylamide gels containing 1× Tris-glycine-EDTA buffer. The gel was dried and exposed to BAS2000 (Fujifilm, Tokyo, Japan). DN, dominant negative; IB, immunoblotting

ments (Fig. 5a). To investigate whether NF-κB binds to regulatory DNA elements, GMSA was performed using nuclear extracts of 3T3-L1 adipocytes. GMSA revealed nuclear protein extracts from BSO-treated 3T3-L1 adipocytes to contain activated NF-κB (Fig. 5b, lanes 1 and 2). The band shift was inhibited by unlabelled oligonucleotide corresponding to a DNA-binding sequence (Fig. 5b, lane 3). In BSO-treated cells, the NF-κB-oligonucleotide complex underwent a supershift in the presence of antibodies against the p65 subunit of NF-κB, indicating that binding to the oligonucleotide is NF-κB-specific (Fig. 5b, lane 4). In 3T3-L1 adipocytes overexpressing the dominant negative IκB, the band shift was also inhibited (Fig. 5b, lane 5). These results suggest that BSO treatment induces NF-κB translocation and that the dominant negative IκB blocks NF-κB pathway activation.

We next examined the effect of the dominant negative IκB on BSO-induced insulin resistance. Insulin-induced glucose uptake was decreased by BSO treatment, while dominant negative IκB overexpression reversed this decrease (Fig. 6a). Reduction of insulin-induced GLUT4 translocation by BSO administration was also reversed by overexpression of the dominant negative IκB (Fig. 6b). BSO treatment decreased insulin-induced IRS-1 phosphorylation and IRS-1-associated p85 and PI 3-kinase activity in the LDM fraction (Fig. 6c, lower panels), but not in whole cell lysates (Fig. 6c, upper panels). However, overexpression of the dominant negative IκB reversed the BSO-induced decreases in IRS-1 phosphorylation and IRS-1-associated p85 and PI 3-kinase activity in the LDM fraction. These results suggest that oxidative stress induces insulin resistance by impairing the normal subcellular distribution of PI 3-kinase, and that the NF-κB pathway is involved in this process.

Discussion

In this study we employed BSO, a glutathione synthase inhibitor, to induce oxidative stress in rats and in 3T3-L1 adipocytes. BSO specifically inhibits the first step of glutathione synthesis and decreases glutathione, an important component of the antioxidant defence system [14]. In fact, we confirmed a decreased hepatic glutathione content and an increased plasma lipid hydroperoxide level, indicating increased oxidative stress in BSO-treated rats. Body weight was lower in BSO-treated rats than in controls, which is consistent with a previous report [35]. BSO-treated rats were apparently insulin-resistant, as demonstrated by a hyperinsulinaemic-euglycaemic clamp study and glucose transport assay using isolated skeletal muscle and adipocytes. These results strongly support the hypothesis that increased oxidative stress can lead to insulin resistance in vivo. Although fasting insulin levels were not elevated in BSO-treated rats as compared with controls, we found that among well-fed animals, insulin levels were significantly higher in BSO-treated rats than in controls. Data from the euglycaemic-hyperinsulinaemic clamp study, along with the observed glucose uptake into isolated tissues and insulin levels in well-fed animals, support the

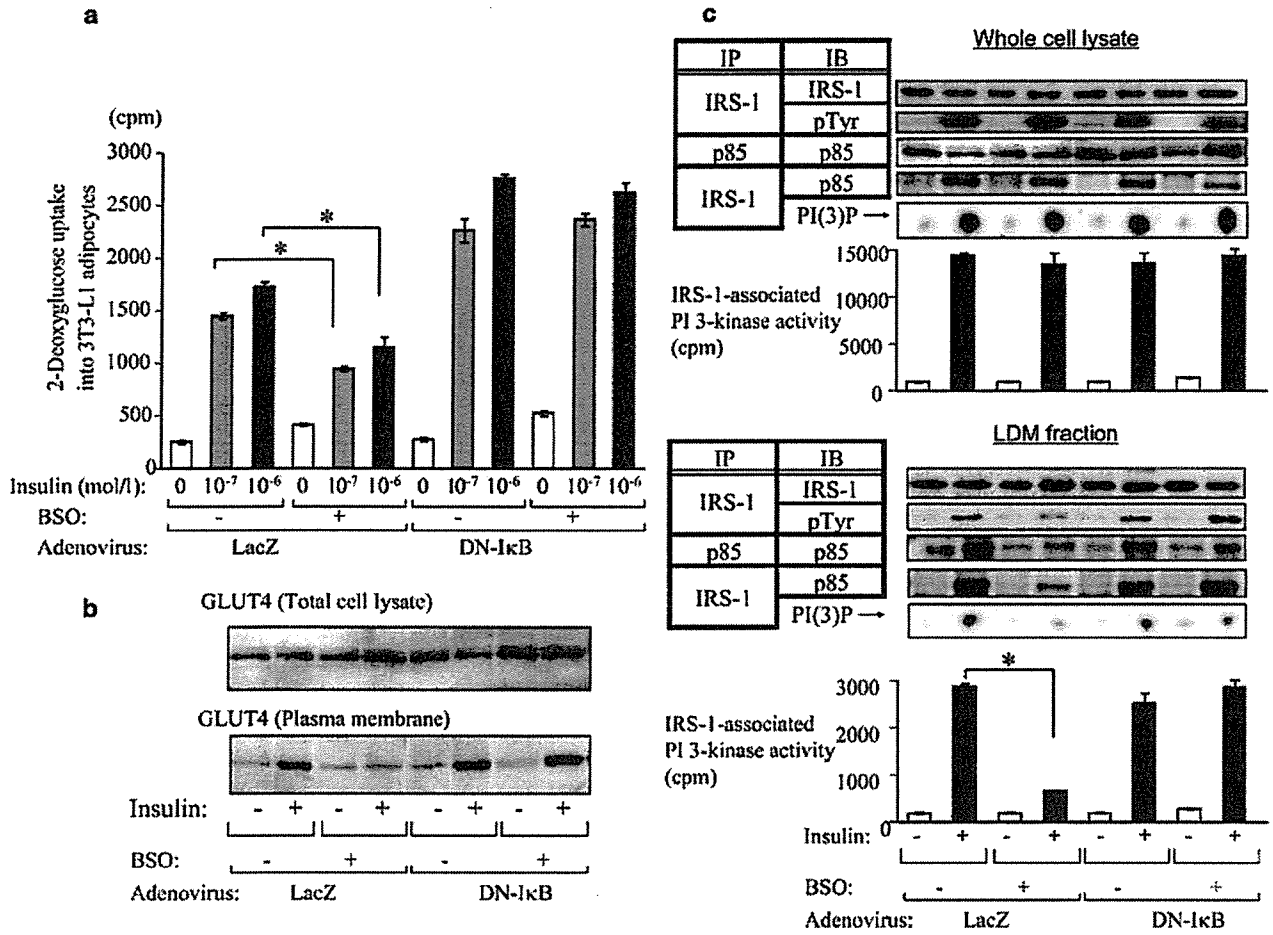

Fig. 6. Effect of dominant negative mutant of IκB on insulin action and insulin signalling in BSO-treated 3T3-L1 adipocytes. **a.** Insulin-induced 2-deoxy glucose uptake into 3T3-L1 adipocytes. Cells overexpressing LacZ (control) and the dominant negative (DN)-IκB adenovirus with or without 80 μmol/l BSO for 18 h were stimulated were stimulated with 0, 10^{-7} or 10^{-6} mol/l insulin for 15 min. Glucose uptake into 3T3-L1 adipocytes was assayed as described in Materials and methods. Bars depict means ± SE of results obtained independently in triplicate. ** $p<0.05$ compared to insulin-stimulated (10^{-7} and 10^{-6} mol/l respectively) control (non BSO-treated) cells. **b.** Recruitment of GLUT4 to the plasma membrane in 3T3-L1 adipocytes overexpressing LacZ and DN-IκB adenovirus with or without BSO pretreatment. The cell lysates and plasma membrane fraction were immunoblotted with anti-GLUT4 antibody. **c.** IRS-1 tyrosine phosphorylation, p85 protein amount and IRS-1-associated PI 3-kinase in whole cell lysates (upper panels) and the LDM fraction (lower panels) of 3T3-L1 adipocytes overexpressing LacZ and DN-IκB adenovirus with or without BSO pretreatment. 3T3-L1 adipocytes were serum-starved for 18 h, pre-incubated with or without 80 μmol/l BSO for 18 h, then stimulated with or without 10^{-6} mol/l insulin for 15 min. Representative immunoblots and representative spots of PI(3)P, independently obtained in triplicate, are shown and bars depict means ± SE of PI 3-kinase activity measured in three independent assays. * $p<0.05$ compared with insulin-stimulated control (non BSO-treated) cells. IB, immunoblotting; IP, immunoprecipitation

conclusion that BSO-treated rats are insulin-resistant. In our experiments, we did not observe the occurrence of overt diabetes with BSO administration, suggesting that this insulin resistance is relatively mild.

A previous report showed no significant difference between BSO-injected rats and controls in terms of insulin-stimulated glucose transport into skeletal muscle [15]. The results of their study contradict our present data demonstrating BSO-induced insulin resistance. We speculate that these different results are attributable to the doses of BSO administered. According to our water consumption data, intake of BSO in BSO-treated rats was approximately 3.5 mmol·kg^{-1} body weight·day^{-1} in the current study. This is a rather high dose compared with the previous report (2 mmol·kg^{-1} body weight·day^{-1}) [15]. Also, the extent of the glutathione decrease was greater in our experiment than in the previous one. In addition, because the previous study did not employ the hyperinsulinaemic-euglycaemic clamp method [15], we believe our picture of insulin resistance in BSO-treated rats to be more accurate.

Insulin-induced IRS phosphorylation and PI 3-kinase activation constitute a critical step in insulin actions such as GLUT4 translocation and glucose uptake [36]. Most insulin-resistant models have been shown

to have impaired insulin-induced PI 3-kinase activation [28, 37, 38]. However, in the BSO-treated rats used in the current study, neither insulin-induced IRS tyrosine phosphorylation nor PI 3-kinase activation in whole tissue lysates of skeletal muscle and adipose tissue were impaired, despite the presence of insulin resistance. In addition, BSO treatment markedly impaired insulin-induced glucose uptake into 3T3-L1 adipocytes and GLUT4 translocation, while insulin-induced IRS-1 tyrosine phosphorylation and IRS-1-associated PI 3-kinase activation were unchanged in whole cell lysates of BSO-treated 3T3-L1 adipocytes. A previous report showed H_2O_2 exposure of 3T3-L1 adipocytes to inhibit insulin-induced glucose uptake, while having no effects on IRS-1 phosphorylation and PI 3-kinase activation [39]. Furthermore, we previously reported chronically angiotensin-II-infused rats, in which plasma lipid hydroperoxide levels were increased, to be highly insulin-resistant, although insulin-induced IRS-1 phosphorylation and PI 3-kinase activation in skeletal muscle and adipose tissue were not impaired [12]. Thus, insulin resistance with normal insulin-induced PI 3-kinase activation in the whole cell may be a common feature in the models with increased oxidative stress.

Regarding the molecular mechanism of this type of insulin resistance, we consider it necessary to examine the possibility of abnormalities in the subcellular distribution of PI 3-kinase. This is based on several reports showing IRS-1 phosphorylation and PI 3-kinase activation specifically in the LDM fraction, though not in whole cell lysates, to be important for insulin action [30, 31]. We speculate that the insulin-induced increase in IRS-1 phosphorylation in the LDM fraction leads to recruitment of the p85 subunit for PI 3-kinase to that fraction. Previous reports have shown that H_2O_2 exposure reduces IRS-1 tyrosine phosphorylation and PI 3-kinase activation in the LDM fraction in 3T3-L1 adipocytes [39, 40]. In the current study, insulin-induced IRS-1 tyrosine phosphorylation in the LDM fraction was demonstrated to be significantly decreased in both BSO-treated rat muscle and adipose tissues and in BSO-treated 3T3-L1 cells. We showed clearly that insulin induces p85 translocation from the cytosol to the LDM fraction in rat muscle, adipose tissue and 3T3-L1 cells and that BSO treatment disrupts this process. Taking our results and those of previous reports together, we consider this disruption of the normal subcellular redistribution of PI 3-kinase to be one of the important mechanisms underlying oxidative-stress-induced insulin resistance.

The activation of transcription factor NF-κB has been shown to be a target of oxidative stress [33]. For example, direct exposure to oxidants such as H_2O_2 activates NF-κB [41], while NF-κB activation can be inhibited by addition of antioxidants such as a vitamin E derivative [42] and lipoic acid [43]. To clarify the contribution of NF-κB cascade activation to oxidative-stress-induced insulin resistance, we utilised the dominant negative IκB. This mutant is a degradation-resistant form of IκB that prevents NF-κB from translocating into the nucleus and is widely used to block cytokine-induced NF-κB activation [44]. Indeed, we confirmed that this mutant is not degraded by TNF-α and that BSO stimulation blocks NF-κB from translocating into the nucleus. Blocking the NF-κB cascade by overexpressing dominant negative IκB had a preventive effect against the decrease in insulin-induced glucose uptake and GLUT4 translocation caused by BSO treatment in 3T3-L1 adipocytes. We observed higher glucose uptake in dominant negative IκB-overexpressing cells than in LacZ control cells. We suggest a possible explanation: dominant negative IκB inhibits the effects of a small amount of inflammatory cytokines secreted by adipocytes. In addition, BSO-induced decreases in IRS-1 tyrosine phosphorylation in the LDM fraction and recruitment of PI 3-kinase to that fraction were also normalised. These results suggest that NF-κB activation is involved in the impaired subcellular redistribution of PI 3-kinase and the insulin resistance induced by BSO treatment.

The precise mechanism linking NF-κB activation and abnormal subcellular redistribution of PI 3-kinase remains unclear. One possible mechanism of inhibited insulin signalling involves NF-κB-activated transcription of inflammatory cytokines such as TNF-α and interleukin-6. NF-κB plays an important role in regulating inflammatory responses [45, 46] and activation of NF-κB may induce inappropriate inflammatory responses, possibly disrupting insulin signalling. Alternatively, PI 3-kinase activation is reportedly necessary for NF-κB activation [47, 48]. Aberrant NF-κB activation may disrupt the PI 3-kinase pathway via a negative feedback mechanism. An anti-inflammatory agent, salicylate, which stabilises IκB via inhibition of IKK and suppression of NF-κB activation, was shown to restore lipid-induced insulin resistance [49, 50]. Because IKK reportedly induces serine phosphorylation of IRS-1, it is possible that BSO activates IKK, resulting in down-regulation of IRS-1 tyrosine phosphorylation in the LDM fraction and impairment of PI 3-kinase recruitment to the LDM fraction.

In summary, our results suggest that oxidative stress induces insulin resistance by impairing insulin-induced IRS-1 phosphorylation in the LDM fraction and subcellular redistribution of PI 3-kinase, and that NF-κB activation is involved in this process. Our present study provides evidence that the NF-κB pathway plays a role in the pathogenesis of oxidative-stress-induced insulin resistance. Judging from our results and those of previous studies, strategies designed to limit inappropriate activation of NF-κB may be an effective approach to treating insulin resistance.

Acknowledgements. The dominant negative mutant of IκB was kindly provided by Dr Richard Gaynor (University of Texas Southwestern Medical Center at Dallas, Tex., USA). The authors are indebted to Naomasa Kakiya of the University of Tokyo for assistance in various areas of this study.

References

1. Betteridge DJ (2000) What is oxidative stress? Metabolism 49 [Suppl 1]:3–8
2. Reaven GM, Lithell H, Landsberg L (1996) Hypertension and associated metabolic abnormalities—the role of insulin resistance and the sympathoadrenal system. N Engl J Med 334:374–381
3. Tuck ML (1990) Metabolic considerations in hypertension. Am J Hypertens 3:355S–365S
4. Baynes JW (1991) Role of oxidative stress in development of complications in diabetes. Diabetes 40:405–412
5. Paolisso G, D'Amore A, Volpe C et al. (1994) Evidence for a relationship between oxidative stress and insulin action in non-insulin-dependent (type II) diabetic patients. Metabolism 43:1426–1429
6. Jones AF, Winkles JW, Jennings PE et al. (1988) Serum antioxidant activity in diabetes mellitus. Diabetes Res 7:89–92
7. Paolisso G, Di Maro G, Pizza G et al. (1992) Plasma GSH/GSSG affects glucose homeostasis in healthy subjects and non-insulin-dependent diabetics. Am J Physiol 263:E435–E440
8. Paolisso G, Balbi V, Volpe C et al. (1995) Metabolic benefits deriving from chronic vitamin C supplementation in aged non-insulin dependent diabetics. J Am Coll Nutr 14:387–392
9. Paolisso G, Di Maro G, Galzerano D et al. (1994) Pharmacological doses of vitamin E and insulin action in elderly subjects. Am J Clin Nutr 59:1291–1296
10. Rajagopalan S, Kurz S, Munzel T et al. (1996) Angiotensin II-mediated hypertension in the rat increases vascular superoxide production via membrane NADH/NADPH oxidase activation. Contribution to alterations of vasomotor tone. J Clin Invest 97:1916–1923
11. Schnackenberg CG, Wilcox CS (1999) Two-week administration of tempol attenuates both hypertension and renal excretion of 8-Iso prostaglandin f2alpha. Hypertension 33:424–428
12. Ogihara T, Asano T, Ando K et al. (2002) Angiotensin II-induced insulin resistance is associated with enhanced insulin signalling. Hypertension 40:872–879
13. Shimosawa T, Ogihara T, Matsui H et al. (2003) Deficiency of adrenomedullin induces insulin resistance by increasing oxidative stress. Hypertension 41:1080–1085
14. Meister A (1983) Selective modification of glutathione metabolism. Science 220:472–477
15. Khamaisi M, Kavel O, Rosenstock M et al. (2000) Effect of inhibition of glutathione synthesis on insulin action: in vivo and in vitro studies using buthionine sulfoximine. Biochem J 349:579–586
16. Vaziri ND, Wang XQ, Oveisi F, Rad B (2000) Induction of oxidative stress by glutathione depletion causes severe hypertension in normal rats. Hypertension 36:142–146
17. Ogihara T, Asano T, Ando K et al. (2001) Insulin resistance with enhanced insulin signalling in high-salt diet-fed rats. Diabetes 50:573–583
18. Yamamoto Y (1994) Chemiluminescence-based high-performance liquid chromatography assay of lipid hydroperoxides. Methods Enzymol 233:319–324
19. Anderson ME (1985) Determination of glutathione and glutathione disulfide in biological samples. Methods Enzymol 113:548–555
20. James DE, Burleigh KM, Kraegen EW (1986) In vivo glucose metabolism in individual tissues of the rat. Interaction between epinephrine and insulin. J Biol Chem 261:6366–6374
21. Hansen P, Gulve EA, Holloszy JO (1994) Suitability of 2-deoxyglucose for in vitro measurement of glucose transport activity in skeletal muscle. J Appl Physiol 76:979–985
22. Rodbell M (1964) Metabolism of isolated fat cells. I. Effects of hormones on glucose metabolism and lipolysis. J Biol Chem 239:375–380
23. Olefsky JM (1975) Effect of dexamethasone on insulin binding, glucose transport, and glucose oxidation of isolated rat adipocytes. J Clin Invest 56:1499–1508
24. Fujishiro M, Gotoh Y, Katagiri H et al. (2001) MKK6/3 and p38 MAPK pathway activation is not necessary for insulin-induced glucose uptake but regulates glucose transporter expression. J Biol Chem 276:19800–19806
25. Katagiri H, Asano T, Ishihara H et al. (1996) Overexpression of catalytic subunit p110alpha of phosphatidylinositol 3-kinase increases glucose transport activity with translocation of glucose transporters in 3T3-L1 adipocytes. J Biol Chem 271:16987–16990
26. Asano T, Kanda A, Katagiri H et al. (2000) p110beta is up-regulated during differentiation of 3T3-L1 cells and contributes to the highly insulin-responsive glucose transport activity. J Biol Chem 275:17671–17676
27. Satoh S, Nishimura H, Clark AE et al. (1993) Use of bismannose photolabel to elucidate insulin-regulated GLUT4 subcellular trafficking kinetics in rat adipose cells. Evidence that exocytosis is a critical site of hormone action. J Biol Chem 268:17820–17829
28. Anai M, Funaki M, Ogihara T et al. (1998) Altered expression levels and impaired steps in the pathway to phosphatidylinositol 3-kinase activation via insulin receptor substrates 1 and 2 in Zucker fatty rats. Diabetes 47:13–23
29. Sakoda H, Ogihara T, Anai M et al. (1999) No correlation of plasma cell 1 overexpression with insulin resistance in diabetic rats and 3T3-L1 adipocytes. Diabetes 48:1365–1371
30. Anai M, Ono H, Funaki M et al. (1998) Different subcellular distribution and regulation of expression of insulin receptor substrate (IRS)-3 from those of IRS-1 and IRS-2. J Biol Chem 273:29686–29692
31. Kriauciunas KM, Myers MG Jr, Kahn CR (2000) Cellular compartmentalization in insulin action: altered signaling by a lipid-modified IRS-1. Mol Cell Biol 20:6849–6859
32. Lu B, Ennis D, Lai R et al. (2001) Enhanced sensitivity of insulin-resistant adipocytes to vanadate is associated with oxidative stress and decreased reduction of vanadate (+5) to vanadyl (+4). J Biol Chem 276:35589–35598
33. Schreck R, Albermann K, Baeuerle PA (1992) Nuclear factor kappa B: an oxidative stress-responsive transcription factor of eukaryotic cells (a review). Free Radic Res Commun 17:221–237
34. Siebenlist U, Franzoso G, Brown K (1994) Structure, regulation and function of NF-kappa B. Annu Rev Cell Biol 10:405–455
35. Leeuwenburgh C, Ji LL (1995) Glutathione depletion in rested and exercised mice: biochemical consequence and adaptation. Arch Biochem Biophys 316:941–949
36. Czech MP (1995) Molecular actions of insulin on glucose transport. Annu Rev Nutr 15:441–471

37. Saad MJ, Folli F, Kahn JA, Kahn CR (1993) Modulation of insulin receptor, insulin receptor substrate-1, and phosphatidylinositol 3-kinase in liver and muscle of dexamethasone-treated rats. J Clin Invest 92:2065–2072
38. Cusi K, Maezono K, Osman A et al. (2000) Insulin resistance differentially affects the PI 3-kinase- and MAP kinase-mediated signalling in human muscle. J Clin Invest 105:311–320
39. Rudich A, Tirosh A, Potashnik R, Hemi R, Kanety H, Bashan N (1998) Prolonged oxidative stress impairs insulin-induced GLUT4 translocation in 3T3-L1 adipocytes. Diabetes 47:1562–1569
40. Tirosh A, Potashnik R, Bashan N, Rudich A (1999) Oxidative stress disrupts insulin-induced cellular redistribution of insulin receptor substrate-1 and phosphatidylinositol 3-kinase in 3T3-L1 adipocytes. A putative cellular mechanism for impaired protein kinase B activation and GLUT4 translocation. J Biol Chem 274:10595–10602
41. Schreck R, Rieber P, Baeuerle PA (1991) Reactive oxygen intermediates as apparently widely used messengers in the activation of the NF-kappa B transcription factor and HIV-1. EMBO J 10:2247–2258
42. Suzuki YJ, Packer L (1993) Inhibition of NF-kappa B activation by vitamin E derivatives. Biochem Biophys Res Commun 193:277–283
43. Sen CK, Packer L (1996) Antioxidant and redox regulation of gene transcription. FASEB J 10:709–720
44. Yamamoto Y, Gaynor RB (2001) Therapeutic potential of inhibition of the NF-kappaB pathway in the treatment of inflammation and cancer. J Clin Invest 107:135–142
45. Baeuerle PA, Henkel T (1994) Function and activation of NF-kappa B in the immune system. Annu Rev Immunol 12:141–179
46. Barnes PJ, Karin M (1997) Nuclear factor-kappaB: a pivotal transcription factor in chronic inflammatory diseases. N Engl J Med 336:1066–1071
47. Sizemore N, Leung S, Stark GR (1999) Activation of phosphatidylinositol 3-kinase in response to interleukin-1 leads to phosphorylation and activation of the NF-kappaB p65/RelA subunit. Mol Cell Biol 19:4798–4805
48. Reddy SA, Huang JH, Liao WS (2000) Phosphatidylinositol 3-kinase as a mediator of TNF-induced NF-kappa B activation. J Immunol 164:1355–1363
49. Kim JK, Kim YJ, Fillmore JJ et al. (2001) Prevention of fat-induced insulin resistance by salicylate. J Clin Invest 108:437–446
50. Yuan M, Konstantopoulos N, Lee J et al. (2001) Reversal of obesity- and diet-induced insulin resistance with salicylates or targeted disruption of Ikkbeta. Science 293:1673–1677